UNIVERSITY OF CALIFORNIA SAN DIEGO

Dynamics of Biogenic Silica in a Coastal Upwelling Filament in the California Current Ecosystem

A thesis submitted in partial satisfaction of the
requirements for the degree Master of Science

in

Oceanography

by

Kayleen Fulton

Committee in charge:

Professor Katherine Barbeau, Chair
Professor Andrew Allen
Professor Michael Landry

2019

The thesis of Kayleen Fulton is approved, and it is acceptable in quality and form for publication on microfilm and electronically:

_____

_____

_____
Chair

University of California San Diego

2019

TABLE OF CONTENTS

ACKNOWLEDGEMENTS

I'd like to thank Kathy Barbeau, my advisor and the chair of my committee, for her support and guidance throughout this work.

Jeff Krause provided many helpful comments and suggestions on my research and his animated willingness to lend his expertise and his enthusiasm about my dataset were very appreciated. I'm also grateful to other students in the Barbeau Lab, Kiefer Forsch, Lauren Manck and Angel Ruacho – all were crucial in all the work that I did, in cruise preparation, learning new techniques, navigating the lab, and staying occupied on ships with many, many games of Euchre. All data collection from the P1706 cruise was a collaborative effort and I could not have done any of it alone.

Our Fe analysis was set up by Kiefer Forsch, and his work and expertise in Fe measurements allowed us to get Fe data complimentary to my bSi data. He contributed his ADCP calculations to be able to make our rough bSi advective flux estimations, and was, in general, a wonderful sounding board for trying to make sense of our datasets. bSi samples from sediment traps were collected by Mike Stukel, who sent them to me to run, and complimentary POC data was contributed by Mike. Pigment data was collected, analyzed and contributed by Ralf Goericke's group. 18S data was provided by Sara Rivera. I also must thank Elizabeth 'Pooh' Venrick, for her help in identifying diatoms under a microscope because, as a chemist, I had never used a microscope before and it was very new territory for me. Andy Allen and Mike Landry were generous to lend their time being on my committee, and I thank them for that.

This thesis is coauthored with Kiefer Forsch, Sara Rivera, Jeffrey W. Krause, Michael R. Stukel, Ralf Goericke and Katherine A. Barbeau. The thesis author was the primary author of this material.

ABSTRACT OF THE THESIS

Dynamics of Biogenic Silica in a Coastal Upwelling Filament in the California Current Ecosystem

by

Kayleen Fulton

Master of Science in Oceanography

University of California San Diego, 2019

Professor Katherine Barbeau, Chair

This study of an upwelling cross-shore filament in the California Current System attempts to follow a parcel of water from upwelling source to offshore in order to characterize changes in silica cycling and associated impacts on carbon cycling under the influence of iron limitation. Water column samples were collected throughout the euphotic zone in conjunction with sediment traps following the filament in Lagrangian fashion (cycles); additional samples were taken across the filament (transects). The filament progressed from iron-replete to iron-limited throughout the study, identified by low silicic acid to nitrate ratios (Si:N) and elevated

nitrate to iron (N:Fe) ratios in situ. Increases in biogenic silica to POC ratios (bSi:POC) in the water column were apparent with increasing iron limitation of the diatom-dominated community. The Lagrangian nature of the study improves overall understanding of the dynamics of biogenic silica as an upwelling filament develops to iron-limited, low Si:N water conditions. This work builds upon and adds context to previous studies which have shown that iron limitation affects silicic acid to carbon (Si:C) and silicic acid to nitrate (Si:N) uptake ratios in marine diatoms. These ratios have potential implications for both carbon and silica cycling in the ocean, impacting uptake and export of these elements. The filament was shown to transport biogenic silica laterally away from the coast, and enhanced silica ballasting was shown to be associated with increased export efficiency offshore.

1. Introduction

The California Current is the eastern limb of the large, clockwise circulation of the subtropical gyre of the North Pacific Ocean. The California Current System off central and southern California consists of the broad, eddy-rich, southward flowing California Current (CC), a persistent but variable subsurface California Undercurrent (CUC) centered on the continental slope that carries water of tropical origin poleward, and a circulation over and near the continental shelf that is energetic and highly seasonal, shifting from a wind-driven equatorward flow and coastal upwelling in spring-summer to poleward flow in fall-winter (Hickey 1998).

A characteristic Eastern Boundary Upwelling System (EBUS), the California Current System experiences summertime equatorward winds that favor coastal upwelling of cold, dense, nutrient-rich water, resulting in areas of high primary production (Carr & Kearns, 2003; Checkley & Barth, 2009). Controls on production in EBUSs are especially of interest because despite the small spatial area that EBUSs occupy in the ocean (<1%), they host nearly 20% of global marine fish catch because of their high primary production (Carr, 2002).

Nutrient-replete conditions in upwelling waters in the California Current region, which typically have ~20% more silicate than nitrate (Zentara & Kamykowski, 1977) generally result in diatom-dominated community blooms (Van Oostende et al., 2015). Diatoms are an abundant type of phytoplankton whose key characteristics include their siliceous shells (frustules) and the critical role they play in oceanic primary production; they fix as much carbon as all terrestrial rain forests and account for up to 40% of all marine carbon export (Field et al., 1998; Marchetti & Cassar, 2009; Martin-Jézéquel et al., 2000; Nelson et al., 1995). The density of silica in diatom frustules offers a degree of mechanical protection as defense (Wilken et al., 2011; Zhang et al., 2017) that can result in reduced grazing. Frustules also play a role in mineral ballasting of

organic material; because they are denser than seawater, they ballast sinking aggregates and fecal pellets. A portion of this carbon sinks to the seafloor and is sequestered. For both of these reasons, diatoms are major exporters of both silica and organic carbon (Smetacek, 1999; Timmermans et al., 2004). Factors that affect diatoms' nutrient uptake, growth, sinking rates, and remineralization rates can have major impacts on nutrient cycling, nutrient sources for pelagic and benthic communities, and carbon sequestration. Further study can help biogeochemical models incorporate these trends to more accurately predict future ocean conditions.

Past studies in upwelling regions have revealed iron supply to be an important bottom-up control on the diatom community (Boyle, 1998; Bruland et al., 2005; Hutchins & Bruland, 1998; Johnson et al., 1999; King & Barbeau, 2007, 2011). Iron (Fe) limits phytoplankton growth in 30-40% of the world's oceans (Moore et al., 2002) and is therefore a major control on oceanic primary production. Fe is a necessary component of microbial growth despite incredibly low concentrations of dissolved Fe in the ocean; while other nutrients exist in micromolar concentrations, Fe is typically available in nanomolar concentrations. Soluble ferrous iron (Fe^{2+}) is rapidly oxidized in oxygenated seawater. Fe limitation has been observed in high production, coastal upwelling regions in EBUSs (Bruland et al., 2001; Firme et al., 2003; Hutchins & Bruland, 1998; Johnson et al., 1999; Biller & Bruland, 2013). Deckboard and in situ bottle amendment experiments in many cases show a rapid response of the diatom community to the addition of Fe.

Fe-related effects on Si biogeochemistry are particularly important in areas of natural Fe limitation. Low-latitude nutrient-replete marine diatoms use dissolved nitrate and silicate, on average, in approximately equal parts (1:1) (Brzezinski, 1985). Under Fe limitation, this drawdown ratio is dramatically affected (Hutchins & Bruland, 1998; Takeda, 1998), being as

high as 4-6 (Franck et al., 2003), and these drawdown ratios can increase cellular Si content (De La Rocha et al., 2000; Leynaert et al., 2004). This has been documented in areas of natural Fe fertilization and in bottle experiments (Brzezinski et al., 2015; Hoffmann et al., 2007; Price, 2005; Takeda, 1998; Twining et al., 2004).

Previous studies have demonstrated changes in diatom nutrient uptake ratios with Fe limitation, and correlations between export efficiency and diatom Fe limitation have been examined in the California Current Ecosystem (CCE) in previous work (Brzezinski et al., 2015; Krause et al., 2015) in a study across fronts during the 2011 CCE Long Term Ecosystem Research (CCE-LTER) cruise. Episodic mesoscale features, such as fronts, eddies and filaments, can move the effects of upwelling-related Fe fertilization events offshore. As upwelling waters flow over the continental shelf, they are enriched from bottom sediments (Bruland et al., 2001) rich in Fe, Fe-binding ligands and organics accumulated from riverine input (Biller et al., 2013; Bundy et al., 2016; Homoky et al., 2012), thought to be the primary source of Fe for upwelling-associated blooms (Johnson et al., 1999). These fluvial inputs accumulate in the benthic boundary layer over the winter season and are brought to the surface with strong spring and summer upwelling. As upwelling water masses age and move offshore, there is a tendency for Fe limiting conditions to develop (Firme et al., 2003; King et al., 2012).

The data presented here is unique in that it attempts to follow the progression of an upwelling filament from recently upwelled and nutrient-replete conditions to Fe-limited in order to gain insight into the changing dynamics of biogenic silica (bSi) as this evolution occurs. Filaments are characteristic of most eastern boundary currents (e.g., Rossi et al., 2013; Sangrà et al., 2015; Stevens & Johnson, 2003). They usually contain a long core of cold water that originates from the upwelled water near the coast. They have cross filament scales of 10-50 km,

and along-filament scales of 50-200 km. The balance of forces within filaments makes them very efficient vehicles for transporting material from upwelling zones to offshore waters, with nutrient-rich conditions enabling growth and fast-moving cores advecting these particulates offshore (e.g., Mohrholz et al., 2014; Muller et al., 2013; Nagai et al., 2015). Mesoscale features such as filaments can contain a predictable primary producer population gradient driven by processes of mixing, nutrient drawdown, and phytoplankton community evolution. They are thus excellent natural laboratories for studying these processes.

The area in this study was chosen because of its characteristic seasonal filaments. The coastline in the Point Conception region makes an abrupt bend to the east to form the Santa Barbara Channel and the Southern California Bight (SCB). A cool pool often forms between Point Conception and Point Arguello to the north (Sverdrup 1938) when upwelled waters to the north meet waters flowing northward along the coast of the SCB (Barth & Brink, 1987; Winant, Alden, et al., 2003; Winant, Dever, et al., 2003). Where these currents meet, a cold filament forms and propagates 10s of km offshore toward the west or southwest before turning S or SE where it can be tracked for hundreds of km (Centurioni et al., 2008; Drake et al., 2011; Kim et al., 2011). These mesoscale features allow for in situ observation of developing Fe limitation on diatoms carried offshore from areas of cool, nutrient-rich, upwelling waters. This thesis focuses on the hypothesis that as nutrient-replete upwelling waters were entrained into a filament and drawn offshore, changes in the cellular composition of diatoms in the filament would show a higher biogenic silica to particulate organic carbon (bSi:POC) ratio with the development of Fe limitation and that a decreasing Si:N signature in the water mass would reflect those changing conditions. We also hypothesized that the development of Fe limiting conditions would increase organic carbon export efficiency offshore from the shelf.

2. Methods

2.1. Study site (Figure 1)

Fieldwork was performed aboard the R/V Roger Revelle between 3 June and 30 June, 2017. To evaluate the hydrographic conditions, an initial SeaSoar survey and a ship-mounted Acoustic Doppler Current Profiler (ADCP) profiling was conducted in an area extending from Pt. Conception in the south to Pt. Pinos in the north, to ~260 m depth and out to ~140 km distance offshore, in four parallel lines spaced ~30 km apart. From this initial survey, a cold-water upwelling filament moving offshore was identified for study. Similar to previous CCE process studies (Landry et al., 2009), four Lagrangian studies of this filament (termed cycles) followed the evolution of the water mass by deploying floating drift arrays and sediment traps, with a holey sock drogue centered at 15 m depth, at the beginning of each cycle for a period of 2-4 days. Locations for the beginning of each cycle were chosen based on Spray glider and remote sensing data and a survey by Moving Vessel Profiler to a depth of 200 m. In addition to the cycles, one sediment trap drift array was deployed at the end of Cycle 2, drifting while Cycle 3 was conducted elsewhere and was retrieved after the end of Cycle 3. Cycle 4 began where this sediment trap ('R2') was retrieved. For each cycle, in situ profile samples were collected once per day around noon for the duration of the cycle, and additional sampling was performed with the trace metal rosette for dFe sampling and obtaining water for Fe-addition grow-out experiments. C1, C2, C3 and C4 were three, four, three and two days in duration, respectively. Cross-filament snapshots were also achieved by sampling in a line perpendicular to the flow of the filament ('Transects'), capturing the structure and bounds of the filament.

2.2. Estimating bSi advective flux

We used high-resolution data acquired by ship-based ADCP in order to estimate the zonal flux (J_u) of bSi in the off-shore flowing filament. The horizontal current determined by ADCP from a moving ship can be prone to masking by tidal currents, turbulence and other small-scale flows (Foreman and Freeland, 1991). In order to analyze flow patterns of the filament, it is necessary to remove these interference signals. Our first approach was to spatially average ADCP profiles over 0.01 degrees of latitude and longitude around a transect bSi profile. We then calculated depth-average horizontal velocity measurements 10 m above and below a bSi concentration data point. We multiplied discrete measurements of bSi concentration by the zonal velocity measurements and averaged J_u across all points contained within the filament core, as well as across the entire transect. Before the velocity vector u and concentration data were multiplied to estimate J_u, we necessarily defined the boundaries of the filament.

In order to determine the lateral and vertical structure of the filament, we used Ocean Data View (ODV) graphing software to plot sections of interpolated potential temperature, chlorophyll (chl-a), and derived buoyancy frequency (N), which is a measure of the stability of the water column or degree of stratification. We assumed the filament was a productive surface feature and contained "memory" of its upwelled water mass source, namely its relatively cold temperature. This analysis was applied to Transects 1 and 2 since the filament water parcel properties were considered heavily modified at Transect 3.

2.3. In situ samples

During cycles and transects, profiles for bSi, macronutrients, chl-a and POC were collected as whole seawater from Niskin bottles once per day at 11 a.m. Trace metal clean samples for dissolved Fe concentration (dFe) were taken using Teflon-coated X-Niskin bottles

on a powder-coated rosette, deployed on a coated hydrowire. Fe samples were handled in a Class 100 trace metal clean van and filtered in-line using acid-washed Teflon tubing and acid-washed 0.2 μm Acropak-200 capsule filters pressurized by filtered air. Filtered samples were acidified to pH 1.8 with hydrochloric acid and stored in 250 acid-clean LDPE bottles for on-shore analysis (Stukel et al., 2017).

2.4. Fe addition grow-out incubations

Incubation studies used seawater from trace metal clean whole seawater samples collected from estimated chl-a max depth. Samples were incubated in acid-cleaned polycarbonate bottles with unamended controls and +Fe (5 nmol·L^{-1} $FeCl_3$) treatments, with three replicates of each. On-deck incubations were run in flow-through incubators screened to 30% light levels for 3-4 days in 2.7 L bottles. On-array incubations were run in 1 L bottles attached to the drifter array at a depth within 5 m of the sample collection depth, for a duration of 2-3 days. On-deck and on-array incubation studies were sampled for chl-a, macronutrients and dFe at initial (t_0) and final (t_f) time points, and for bSi, POC and community composition (except C1) at t_f. Additionally, deck incubations were sampled once a day between t_0 and t_f for chl-a and macronutrients. Community composition in incubation samples preserved with 10% buffered formalin was quantified by inverted microscope using the Utermöhl method. Samples were allowed to settle in 25 or 50 mL (depending on concentration) settling chambers for 24 hours before counting.

2.5. Sediment traps

8-12 VERTEX-style particle interceptor traps (PITs) were placed on a sediment trap array at three depths: 150 m, 100 m and the base of the euphotic zone (40 – 60 m, determined by

fluorescence profiles prior to deployment). PITs were 70 mm in diameter, with an 8:1 height to diameter aspect ratio, and a baffle on top consisting of 13 acrylic tubes with a similar 8:1 aspect ratio and tapered ends. Tubes contained a solution made from 0.1-µm filtered seawater amended with 60 g L^{-1} NaCl and 0.4% (final concentration) formaldehyde. Sediment traps were deployed at the beginning of a cycle, collected on the last day of the cycle and averaged over the time spent deployed. (Knauer et al., 1979; Morrow et al., 2018)

2.6. Macronutrient and chl-a analysis

Macronutrient samples were collected from in situ and incubation samples and frozen for on-shore autoanalyzer analysis. Water column nutrient samples were filtered through a 0.1-µm capsule filter before being frozen. Chl *a* samples in dark bottles were filtered onto 25 mm GF/F filters and analyzed on-board the ship, after extraction for 24h in in 90% acetone at -20°C. Chl *a* was quantified using a Turner Designs 10-AU Fluorometer, fitted with a red-sensitive photomultiplier tube.

2.7. Biogenic silica analysis

In situ bSi samples were transferred to 1 L polycarbonate bottles and filtered onto 47 mm 0.6-µm polycarbonate filters, which were then dried in the oven at 60˚C for 24 hours and stored for on-shore analysis. Incubation bSi samples used 400-900 mL seawater, depending on availability, and were filtered and dried similarly. Samples were digested in 4 mL 0.2 N NaOH in HF-clean teflon tubes at 95˚C for 40 minutes and then cooled in an ice bath and neutralized with 1 mL 1 N HCl. After centrifuging 10 min at 1100 x g, 4 mL were withdrawn, diluted and measured at 810 nm for reactive silicate via the colorimetric ammonium molybdate method (Brzezinski & Nelson, 1995; Paasche, 1973; Strickland & Parsons, 1977), where a 10 mL sample

was added to a 4 mL molybdate solution and allowed to stand 10 minutes before being reduced for 2 hours.

2.8. POC analysis

0.5-2 liters of seawater was filtered through pre-combusted 25 mm Whatman GF/F filters under low vacuum pressure. The filter was subsequently wrapped in precombusted aluminum foil and stored in liquid nitrogen until processing. Samples were then placed on combusted petri plates and acidified in a dessicator with HCl fumes, then dried for 48 hours at 60°C. The samples were cut in half, weighed, placed in a tin capsule, and measured on a CHN elemental analyzer at the Scripps Institution of Oceanography Analytical Facility. More information on this method can be found at https://cce.lternet.edu/data/methods-manual/.

2.9. Dissolved Fe analysis

Stored acidified filtered seawater samples were analyzed for Fe using flow injection with chemiluminescence methods and a manifold adapted from Lohan et al., (2006). DFe in the resulting samples was oxidized to iron(III) for 1 h with 10 mM Q-H_2O_2, buffered in-line with ammonium acetate to pH ~3.5 and selectively pre-concentrated on a chelating column packed with a resin (Toyopearl® AF-Chelate-650M). DFe was eluted from the column using 0.14 M HCl and the chemiluminescence is recorded by a photomultiplier tube (Hamamatsu Photonics) (King & Barbeau, 2007, 2011). The standardization of Fe used was a matrix-matched standard curve (0, 0.4, 0.8, 3.2 nmol kg^{-1}) using low-Fe open ocean seawater. Standards were treated identically to samples. Accuracy was assessed by repeated measurements of GEOTRACES coastal and open Pacific Ocean reference seawater samples.

2.10. Molecular Methods for Quantitative Phytoplankton Analysis

RNA was extracted from 0.22 μm sterivex filters (Cat. No. SVGP01050) with a Macherey-Nagel NucleoMag RNA 96 kit (Cat. No. 744350.1). RNA quality was analyzed on an Agilent TapeStation with the RNA ScreenTape system (Cat. No. 5067-5576). Invitrogen SuperScript III Fist-Strand cDNA Synthesis System (Cat. No. 18080051) was employed to make cDNA for all extracted samples using their standard protocol and random hexamers. The first strand cDNA was a template to generate 3 different amplicon libraries for all the samples. 16S V4-V5 rDNA amplicon libraries were made for each sample using 515F (GTGYCAGCMGCCGCGGTAA) and 926R (CCGYCAATTYMTTTRAGTTT) primers, 18S V4 rDNA amplicon libraries were made using EukV4F1 (CCAGCASCYGCGGTAATTCC) and EukV4R1 (ACTTTCGTTCTTGATYR) primers, and 18S V9 rDNA amplicon libraries were made using 1389F (TTGTACACACCGCCC) and 1510R (CCTTCYGCAGGTTCACCTAC) primers. PCR was performed using Azura TruFi DNA Polymerase PCR kit (Cat. No. AZ-1710) following the standard protocol. PCR clean-up was performed using Beckman Coulter AMPure XP beads (Cat. No. A63881) following the standard PCR clean-up protocol. PCR quantification was performed using Invitrogen Quant-iT PicoGreen dsDNA Assay kit (Cat. No. P11496) and evaluated on a FlexStation 3 multimode plate reader. 16S rDNA and 18S rDNA amplicon libraries for all samples were individually barcoded and pooled, respectively. The rDNA amplicon pools were sequenced at UC Davis sequencing core. The 16S rDNA pool was ran on 1 lane of an Illumina PE300 MiSeq, the 18S V4 rDNA amplicon pool was also ran on 1 lane of an Illumina PE300 MiSeq, and the 18S rDNA V9 pool was ran on one lane of an Illumina PE150 MiSeq run. Demultiplexed reads were then quality filtered and subject to swarm OTU clustering and taxonomic classification of small subunit ribosomal ribonucleic acid (SSU rRNA) using John McCrow's rRNA_pipeline (https://github.com/mccrowjp/rRNA_pipeline).

2.11. Phytoplankton pigment analysis

Diatom contribution was estimated using phytoplankton accessory pigments, collected and analyzed as described in Goericke & Montoya, 1998.

2.12. Miscellaneous calculations

Chl-a, macronutrient, bSi and POC values were averaged over the depth of the euphotic zone, which was calculated by fitting the noon-time PAR profiles to a logarithmic best-fit to find the 1% isolume. Vertical trapezoidal integrations were calculated by averaging two depth-adjacent values multiplied by the depth between the samples, and summing the values above the desired depth (above the depth of the euphotic zone or mixed layer). When ratios were calculated using vertically integrated values, standard deviation was calculated using error propagation:

$$\partial R = |R| \times \sqrt{\left(\frac{\partial a}{a}\right)^2 + \left(\frac{\partial b}{b}\right)^2}$$

Cell counting via inverted microscope was calculated according to Karlson et al., (2010):

$$cells\ mL^{-1} = N * \left(\frac{A_t}{A_c}\right) * \frac{1}{V}$$

where V = volume of chamber (mL), A_t = total area of the chamber (mm^2), A_c = counted area of the chamber – transverse threads multiplied by number of fields of view counted (mm^2), and N = number of units counted.

3. Results

3.1. Spatial orientation

Satellite images of sea surface temperature (SST) and Chl-a and data from a Moving Vessel Profiler informed the location for Cycle 1 (C1). Sampling began in a relatively low-temperature, high salinity, high chl-a water mass located over the shelf, with a fast-moving southwestward flow. C2 began off the shelf and within the filament, 71 km southwest from the start-point of C1, just above the Santa Lucia Escarpment. At the end of C2, a sediment trap drift array (R2) was deployed and left for five days while C3 was completed, 135 km southwest of the start-point of C2 (**Figure 1**). C4 began where R2 was retrieved, and therefore should be considered a time-evolved water mass from C2. R2 moved in a c-shape, travelling northwest, then southwest, then turning northeast just before retrieval, suggesting that R2 was entrained into an eddy at the end of C2. C4 sampling was conducted in the northeastward flow.

A Temperature versus Salinity (T-S) plot (**Figure 2**) shows that the signatures of the water masses in Cycles 1, 2 and 4 have similar properties while Cycle 3 diverges from the trend. For this reason, it is likely that the water mass in the latter days of C3 was separate from the filament water. This is supported by density profiles with deeper mixed layers than all other cycles and by Si:N values (**Table 1**) more characteristic of transitional waters. To focus on filament development, data from the latter days of C3 will be discussed in less depth than other data points.

3.2. In situ conditions

Macronutrients were highest on Cycle 1, Day 1 (C1D1), closest to the coast and presumably closest to the beginning of the upwelling filament, with nitrate at 10.53 μM and

silicate at 10.68 μM (**Table 1**). Macronutrients decreased between C1D1 and C1D2. Between C1D2 and C1D3, nitrate remained relatively stable (6.69 μM to 6.42 μM) while silicate continued to decrease slightly (7.11 μM to 5.89 μm). Throughout C1, nutrient profiles show a gradual increase with depth in concentrations throughout the euphotic zone, with maximum gradients (nutricline) occurring at sampling depth midpoints of 6 m (C1D1), 13 m (C1D2) and 26 m (C1D3) (**Figure 3**). C2D1 was higher in nitrate than C1D3 (10.11 μM), and notably more depleted in silicate relative to nitrate (6.72). (**Table 1**). Differences in nutrient ratios and absolute concentrations between C1D3 and C2D1 suggest that the water mass studied in C2 was not directly derived from C1 and may represent a mixture of several different source waters entrained by the filament from the shelf region. Nitrate and silicate concentrations were relatively stable for the first three days of C2, dropping slightly on C2D4. Nutriclines were estimated (by max gradient) to be 15, 25, 25 and 38 m for the respective four sampling days. C3D1 was low in nitrate (3.46 μM) and silicate (3.55 μM) with decreasing values on C3D2 and C3D3, and nutriclines at 88, 68 and 68 m for the respective three sampling days (**Figure 3**). Nitrate and silicate on the first day of C4 (C4D1) were similar (within 1 μM) to the last day of C2 (C2D4) and both days had estimated nutriclines of 45 m.

Water column bSi, POC and Chl-a measurements were highest in C1 and C2, with an increasing trend through C1 and a decreasing trend through C2, with the exception of C2D4, which saw a slight increase in bSi, POC and Chl-a (**Figure 4**). bSi was at its observed maximum for all cycles on C2D1, at 3.15 μM, POC on C1D3, at 41.12 μM and Chl-a on C1D2 at 6.47 μg/L (**Table 1**). Chl-a max was at a depth of 6, 13 and 26 m for the three respective days of C1 and 15, 25, 25 and 38 m for the four respective days of C2 (**Figure 3**). C3 and C4 saw a significant drop in all three values, with average bSi concentrations of 0.61 μM (C3) and 0.28 μM (C4),

POC concentrations of 7.39 μM (C3) and 8.12 μM (C4) and Chl-a concentrations of 1.16 μg/L (C3) and 0.33 μg/L (C4) (**Table 1**).

Because of the inherent difficulty in collecting trace metal clean samples, dFe datapoints are less frequent than other in situ data. dFe (K. Forsch, unpublished data) averaged 1.6 nM over the euphotic zone in C1D1 and, by C1D3, dropped by over half to 0.60 nM and to 0.13 nM by C2D1. Besides a slight increase on C3D1, dFe remained below 0.19 for the remaining duration in this Lagrangian study.

Community composition analysis by 18S (S. Rivera, unpublished data) suggests a dominance of diatoms in C1, with diminishing populations in C2 and C4. Major contributing diatom species in C1 were *Pseudo-nitzschia australis*, *Chaetoceros rostratus* and *Thalassiosira* spp.; in C2, major species included *Chaetoceros radicans* and *Chaetoceros rostratus,* with *Pseudo-nitzschia* spp. in the beginning of the Cycle and disappearing toward the latter half of the Cycle and *Thalassiosira* spp. becoming relatively more abundant on days 2, 3, and 4. C4 had very little biomass, with dominant diatom species being *Thalassiosira* spp.

Estimated diatom contribution by surface pigment analysis show diatoms were between 61% and 73% of the community in stations within the area defined as the filament (§2.1.) in Transect 1 and between 56% and 93% in stations within the area defined as the filament in Transect 2 (**Table 2**).

3.3. Incubations

In incubation samples, direct evidence of Fe stress is apparent from chl-a increases in amended samples, where increases were most apparent in the latter days of C2 and C4 (**Table 3**). The rate of nutrient drawdown in incubations increased from C1 to C2, with complete nutrient

drawdown within 3 days in C1D1 and 24 hours in C2D1 (**Figure 5**). In C1, an apparently Fe replete regime, amended samples showed little difference in either bSi or POC. In all cycles, bSi between control and amended samples showed little difference and, on average, were within 0.13 μM of each other (**Figure 6**). POC values showed more variability, with average absolute differences between conditions of 4.94 μM in C1, 14.79 μM in Cycle 2, 4.05 μM in C3 and 2.65 μM in C4 (**Figure 6**). POC values for amended samples in Cycle 2 and in C4D1 significantly exceeded the control values.

Community composition observed via microscopy is shown for control samples for Cycles 2 and 4 (**Figure 7**) The community composition of C2D1 control incubations were mostly comprised of *Chaetoceros* spp. (546 ± 22 cells mL^{-1}) and *Pseudo-nitzschia* spp. (337 ± 158 cells mL^{-1}). (**Figure 7**). C2D4 and C4D1 control samples showed a similar trend in that diatoms in the < 20 μm category increased, while all other categories showed a significant relative decrease. This presumably reflects differences in the diatom community between cycles, as discussed above base on 18S data. Changes in bSi:POC ratios in incubations were heavily dependent on increased POC in amended samples rather than any increase in bSi, which remained stable with Fe addition. The greatest differences in bSi:POC between control and amended samples were in C2 (**Figure 6c**), with amended samples being significantly lower in bSi:POC than their respective controls.

3.4. Offshore Transport

In Transect 1, outcropping of the 12.5°C isotherm and elevated concentrations of chl-a indicate stations 3-8 are within the loosely defined filament (**Figure 8**). A relatively cold-core feature is still present at Transect 2, indicated by outcropping of the 13.5°C isotherm. Heating of

the filament is expected as it is advected offshore due to insolation of the surface. A broader and more cohesive filament is indicated by elevated concentrations of chl-a (>3 μg L^{-1}). Together, potential temperature and chl-a sections indicate stations 2-8 are within the filament at Transect 2 (**Figure 9**).

We interpret a maximum in N as the lower boundary of the filament, where resistance to vertical displacement is at a maximum (i.e. stability). We find that in Transect 1, N_{max} occurs at 45 m across the filament, whereas it varies from 30 – 50 m in Transect 2. The within-filament zonal flux of bSi increased almost 7-fold between the transects due to increases in both the off-shore velocity of the filament and inventory of bSi (**Table 4**). Averaged across the entire transect, we determined a net negative J_u (westward) for both transects, confirming our hypothesis that filaments are efficient vehicles for lateral transport of suspended biogenic material to the offshore region.

3.5. Export

Sediment traps were deployed and retrieved at the beginning and end of each cycle and flux values are per day averages over the duration of the cycle. Export data were collected at 150 m, 100 m (except R2), and at depths that were estimated, at the time of deployment, to be the base of the euphotic zone (40-60 m). bSi export was highest in C1, followed by C4, and lowest in C3 at all three depths (**Table 5**). At the base of the euphotic zone, POC export was highest in C3 (46.62 mmol m^{-2} d^{-1}) and at 100 and 150 m, in C4 (26.68 and 25.87 mmol m^{-2} d^{-1}, respectively) (**Figure 10**).

4. Discussion

While many studies have been done in EBCs to investigate upwelling, Fe limitation, and the physical characteristics of filaments and export, this study is unique in combining these foci and following the same water mass from upwelling source to offshore. Following the same water mass has its difficulties, as a single water mass can have multiple sources and meander in many different directions. The most definitive time-evolved water masses in this study were Cycles 2, 4 and the sediment trap left to drift between those cycles. The two latter days of Cycle 3 were almost certainly a separate water mass from outside the filament. Cycle 1 and Cycle 2 share characteristics, with a separate upwelling source likely contributing to Cycle 2. This is evidenced by patterns in nutrient concentrations and significantly differing bacterial communities between the two cycles (S. Rivera, unpublished data).

4.1. Fe limiting conditions and macronutrient ratios in an upwelling filament

Areas of potential Fe limitation have been linked with narrow shelf widths and low riverine input (Chase et al., 2007), making this area a likely candidate for potential Fe limitation, especially given that Fe limitation has been shown even with moderate shelf widths in upwelling areas (Till et al., 2019). Another factor that has been found to coincide with potential Fe limitation is whether or not the parcel of water is beyond the shelf break; beyond the shelf break, upwelling systems have been observed to quickly become Fe limited (Till et al., 2019). In this case, C1 was conducted in several hundreds of meters and C2 in several thousands of meters. C1 was found to be Fe replete, and C2 Fe limited. While C2 likely has a separate or additional upwelling source from the parcel in C1, this does provide further evidence for the shelf break being one indicator of potential Fe limitation.

N:dFe ratios > 10-12 can be indicative of a nutrient regime that is likely to become Fe stressed (King & Barbeau, 2007), and C2 and C4 are the only cycles that fall well above this threshold (**Figure 11**). Additionally, Fe limited diatoms preferentially deplete the water of Si over N (Brzezinski et al., 2015; Firme et al., 2003; Franck et al., 2000, 2003; Hutchins & Bruland, 1998; Krause et al., 2015; Leblanc et al., 2005; Takeda, 1998), decreasing in situ Si:N and leaving a compounding signature of Fe limitation. Although it is not possible to quantitatively specify, based on our 18S and microscopy data, the degree to which diatoms dominated the phytoplankton biomass at C1 and C2, the high chl levels at these cycles are characteristic of diatom-dominated communities in the California Current regime (Goericke, 2011; Li et al., 2010) and pigment analysis from the surfaces of Transect 1 and Transect 2 indicate a dominance of diatoms in the phytoplankton community within the filament (**Table 2**). Mixed layer Si:N values decreased significantly in C2 relative to C1 and were consistently low between C2 and C4 (**Figure 11**), this suggests that most of the Fe available was rapidly removed between C1 and C2, resulting in an Fe-stressed diatom community that preferentially depleted Si relative to N in the core of the filament. Rapid and significant growth in response to Fe addition in C2 corroborates the onset of Fe limitation. Diatom response in C4 incubations was less significant, likely due to a dying diatom community. Microscopy samples in C4 were dominated by small, centric diatoms and aggregates with mainly dead or dying specimens that were unlikely to show any significant response to nutrient addition. However, an in situ Si:N signature (**Figure 11**), showing increased Si consumption over N consumption combined with the high export from C4 waters (**Figure 10**), indicates that more Fe-stressed diatoms than observed were likely present and settled out by the time of sampling. Si:N ratios within the filament showed a very different signature than sample points outside the filament, as the latter days of Cycle 3 were determined

to be. High Si:N values in C3D2 and C3D3 (**Table 1**) showed no evidence of Fe limited diatom nutrient uptake. Si:N previously observed off of Point Conception found similar conditions to C2 for Fe limited diatoms during upwelling periods (King & Barbeau, 2011). **Figure 12** shows a clear evolution of diatom Fe stress as surface Si:N increases from C1 to C4 (excluding C3). These data include all cycles, transects and underway surveys to create a more comprehensive surface Si:N map of the area within and surrounding the filament. These geochemical indicators of Fe stress agree with direct evidence of Fe stress from incubation samples which point to C2 and C4 diatom growth being Fe limited, consistent with the hypothesis of the upwelling filament transitioning from nutrient replete to Fe limiting for diatom growth as it moves offshore.

4.2. Impact of Fe limitation on elemental stoichiometry of diatoms

Fe stress affects light harvesting, carbon acquisition, and nitrate assimilation because these are Fe intensive processes (Hutchins & Bruland, 1998; Takeda, 1998). Potential increases in silica accumulation have been attributed to slower growth and progression through the cell cycle (De La Rocha et al., 2000), with increased time spent in M-phase, which is the part of the cell cycle associated with silica deposition (Smith et al., 2016). Increased time spent in this part of the cycle when silica is not limiting in the environment can increase cellular silica content, but even in cases where biogenic silica (bSi) does not increase, reduced nitrate assimilation and carbon acquisition increase Si:N and Si:C uptake and the ratio of bSi to particulate organic carbon (bSi:POC) increases (Marchetti & Harrison, 2007). These changes in cellular composition can affect the efficiency of carbon export and sequestration (Assmy et al., 2013; Brzezinski et al., 2015; Hutchins & Bruland, 1998; Wilken et al., 2011).

Between C1 and C2, bSi:POC (**Figure 11**) trends upward with a sampled maximum of 0.16 µmol:nmol on C2D2. While this trend suggests that diatoms in this nutrient-replete upwelling region entrained into the filament show this change in cellular composition with the development of Fe limitation, it is important to note that both bSi and POC measurements include detritus and contributions from other planktonic organisms. Differences in the remineralization of POC relative to bSi in the euphotic zone may also contribute to this trend. C3D1 and C4 see a consistent decline in bSi:POC, likely with the decline and sinking out of the community. Higher bSi:POC diatoms are likely to sink faster due to their increased ballast, which could contribute to that decline. The data from the latter days of C3 are likely unrelated to the filament. Cycle days grouped by Si:N (**Figure 13**) in a similar fashion as in a CCE study of a frontal region (Brzezinski et al., 2015) show consistency with nutrient-replete (Si:N = 1-2), Fe stressed (Si:N < 1) and transitional/oligotrophic conditions (Si:N > 2). All days from C2 and C4 fit the Si:N < 1 category while C1 fits the Si:N = 1-2 category, with values just under 1 for C1D3, consistent with developing Fe stress. Si:N values for C3D2 and C3D3 are in the Si:N > 2 category. In terms of the three Si:N categories in **Figure 13**, bSi:POC ratios (**Table 1**) reflect changes in water column Si:N, with average bSi:POC values of 0.06 ± 0.017 (Si:N > 2), 0.09 ± 0.018 (Si:N = 1-2) and 0.11 ± 0.047 (Si:N < 1). bSi:POC values in Brzezinski et al., (2015) were similar in the former two categories (~0.01 and ~0.07, respectively), but with an intermediate value for the Si:N < 1 category (~0.04).

Though these CCE mesoscale features in these comparisons are not identical, these values provide useful correlations between in situ nutrient data and bSi:POC ratios in this region. By following these waters from source to offshore, our study substantiates the contention that Fe limitation is an influence on increasing bSi:POC ratios, likely related to cellular changes in

diatom bSi:POC. It is important to note that changes in overall bSi:POC with developing Fe limitation does not necessarily indicate solely physiological changes in diatoms, but could be influenced by changes in community composition as well. For example, small diatoms are often characterized as more lightly silicified than large diatoms (Quéguiner, 2013; Tréguer et al., 2018) and a shift in community composition toward smaller diatoms could result in a lower bSi:POC. In this study, we saw a shift from largely *Chaetoceros* and *Pseudo-nitzschia*, which are both characterized as lightly-silicified 'C-sinkers' (Tréguer et al., 2018), to a more diverse set of small diatoms. The varying contributions of non-diatom planktonic organisms may also influence observed patterns of bSi:POC. While combined microscopy and 18S data gives us a good idea of the relative changes in community composition of diatoms, it does not give us a quantitative figure for the contribution of diatoms to the overall phytoplankton biomass.

Fe addition grow-out incubations were generally carried out for 3 days, as has been typical in Fe limitation studies. In previous studies in the California Current, as well as the Ross Sea, the Humboldt current and the Peru Upwelling (Hutchins et al., 1998, 2002; Hutchins & Bruland, 1998; King & Barbeau, 2007; Sedwick et al., 2000), a 3-4 day incubation timeline has captured nutrient depletion and chl-a increases following Fe addition fairly evenly. However, in the current incubation studies, nutrients in Fe limited areas were depleted following Fe addition much more quickly than previous studies (**Figure 5**). Cycle 1 saw nitrate depletion by day 3, whereas the beginning of the Fe-limited Cycle 2 saw nitrate depleted within the first 24 hours, and later in Cycle 2 between t = 2 and 3. This observed decoupling of nutrient uptake has been observed in and is consistent with previous Fe incubation studies (Hutchins & Bruland, 1998). One implication of this unexpected nutrient uptake rate is that final timepoint snapshots observed by microscopy may not be accurate representations of the community since, by day 3

communities had been in low nutrient conditions for up to 48 hours. These uptake rates may be due to rapid iron and nitrate acquisition strategies by phytoplankton in this EBUS of high flux and rapidly changing conditions.

In a paper studying Fe limitation in aging upwelling water along the Northern California coast, Firme et al., 2003 found that particulate C:N increased with Fe addition in incubation experiments. Data from our incubation studies agree with this finding, however, in situ particulate C:N showed a small increase with increasing Fe limitation within the filament. Ratios in both of these instances (in situ and in incubations) will depend heavily on changing community compositions and, thus, for further elucidation on these trends, studies on changes in particulate C:N due to Fe stress would have to either be closely coupled with detailed analysis of changing community compositions or done on single-species communities.

4.3. Offshore Transport and Export Flux

Averaged across the entire transect, we calculated a net negative J_u (westward) for both transects, confirming our hypothesis that filaments are efficient vehicles for lateral transport of suspended biogenic material to the offshore region. The role that mesoscale features have on the movement of organic matter from coastal to oceanic regions has been increasingly recognized in recent years to have significant impacts on nutrient cycles (e.g. lateral transport, export, and sequestration). A modeling study found filaments to be a 'primary determinant of biological tracers in the coastal region' (Nagai et al., 2015), and another experimental study in the Benguela Current found that the impact of even small filaments was not negligible (Hösen et al., 2016). These findings of increased offshore export due to lateral transport by filaments is consistent

with the observations of high-velocity offshore transport of suspended biogenic material in this filament study.

Despite having lower biomass in the euphotic zone at C4 than any other cycle within the filament, POC export is higher at C4 than all other cycles and bSi is higher than all except C1 in the 100 and 150 m traps (**Table 5**). At 150 m, C1 bSi export is ~8.8% of the inventory whereas at C4 it is ~24.4%, and C1 POC export is 1.5% of the inventory whereas at C4 it is 4.9%. Export for both bSi and POC appears to be more efficient in C4, within the region of Fe stress, than in both C1 where diatoms are Fe-replete, and C2 where diatoms are beginning to experience Fe limitation, supporting findings of increased diatom-mediated POC export in Fe limited California upwelling regimes (Brzezinski et al., 2015). These findings are suggestive of Fe limited diatom influence, though the contribution of diatoms to the overall phytoplankton community is unclear based on these data. The CCE region has been found to be strongly advective (Kelly et al., 2018), which can result in decoupling of production and export, and this decoupling is a phenomenon of meso- and submesoscale features that has been noted in the California Current (Landry et al., 2009; Plattner et al., 2005). Increased export in the offshore, low-biomass stages of the filament is likely due to a combination of lateral transport from higher-biomass stages and of increased ballasting due to Fe limitation of diatom-laden aggregates and fecal pellets. In order to facilitate a better understanding of the relative contribution of these factors, data such as these can contribute to models that incorporate both of these trends and better predict the effects of Fe limitation in these mesoscale features.

5. Conclusions

This study is the first to follow a filament in the California Current from origin to offshore, in a Lagrangian fashion, with a focus on the effects of Fe limitation. A filament was successfully identified, followed in Lagrangian sampling and defined by cross-sectional snapshots. Developing Fe limitation led to a decreasing in situ Si:N signature, correlated with increased bSi:POC ratios. Fe incubation studies showed rapid response in growth in samples from beyond the shelf break, with decreased bSi:POC in previously Fe limited samples. Reduced bSi:POC ratios were primarily due to increased POC content rather than changes in bSi. Pigment analysis suggests that the phytoplankton community was dominated by diatoms within the filament, indicating that the observed trends are likely due to changes in the physiology or community composition of diatoms. Cross-filament transect data showing a high-velocity, high-volume westward transport of biogenic material supports the hypothesis that filaments are an effective vector for moving particulate matter offshore and later stages in the filament showed enhanced offshore export, which is likely a combination of lateral transport of particles and enhanced ballasting of diatoms due to increased bSi:POC ratios. Future studies might combine more species-specific data on changes in diatom communities with these analyses to understand the exact causes for these observed trends.

6. Figures, Tables and Captions

Table 1: Vertically integrated averages in the euphotic zone of in situ conditions

	Euphotic zone (m)	$Si(OH)_4$ (µM)	NO_3 (µM)	$Si(OH)_4$:NO_3 (mol:mol)	bSi (µM)	POC (µM)	bSi:POC (mol:mol)	Chl-a (µg L^{-1})	N:dFe (µmol:nmol)
C1D1	24	10.68	10.53	1.03	2.02	28.69	0.07	4.40	12.70
C1D2	21	7.11	6.69	1.07	2.79	28.38	0.10	6.47	
C1D3	22	5.89	6.42	0.92	2.82	41.12	0.07	5.49	10.61
C2D1	37	6.72	10.11	0.53	3.15	24.85	0.10	5.26	61.12
C2D2	31	6.01	9.78	0.57	2.42	15.21	0.16	3.74	
C2D3	38	6.33	9.58	0.61	2.07	14.09	0.14	2.11	69.99
C2D4	36	4.61	7.95	0.58	2.16	16.37	0.13	2.39	
C3D1	36	3.55	3.46	1.03	1.01	10.20	0.10	1.79	15.07
C3D2	53	3.03	1.51	3.42	0.36	7.10	0.05	0.78	
C3D3	65	2.63	0.68	64.07	0.30	4.61	0.07	0.55	3.92
C4D1	61	5.14	7.03	0.51	0.38	7.70	0.06	0.39	59.16
C4D2	59	4.60	6.60	0.42	0.17	8.64	0.04	0.27	
C1	22	7.89	7.88	1.01	2.54	32.73	0.08	5.45	11.95
C2	35	5.56	9.16	0.54	2.69	20.58	0.13	4.12	65.32
C3	52	2.98	1.93	25.92	0.61	7.39	0.08	1.16	10.44
C4	60	4.87	6.81	0.47	0.28	8.12	0.05	0.33	59.16

Table 2: Phytoplankton biomass estimates (µg chl L^{-1}). Boxed stations are in a zone determined to be within the filament.

Transect	Station	Depth	Dinoflagellates	Diatoms	% of total	Prymnesiophytes	Pelagophytes	Synechococcus	Chlorophytes	Cryptophytes	Prochlorococcus
1	1	2	0.013	0.538	(43%)	0.217	0.008	0.021	0.194	0.275	0.000
1	2	2	0.006	0.917	(63%)	0.202	0.013	0.019	0.124	0.171	0.000
1	3	2	0.086	2.943	(88%)	0.118	-0.006	0.010	0.000	0.192	0.000
1	4	2	0.000	2.391	(73%)	0.191	-0.009	0.012	0.142	0.546	0.000
1	5	2	0.000	1.556	(66%)	0.211	-0.010	0.029	0.161	0.422	0.000
1	6	3	0.000	1.597	(67%)	0.185	-0.009	0.019	0.173	0.406	0.000
1	7	3	0.000	1.204	(61%)	0.201	0.030	0.010	0.164	0.352	0.000
1	8	2	0.000	1.574	(63%)	0.260	0.040	0.031	0.153	0.433	0.000
1	9	3	0.000	2.548	(73%)	0.307	-0.015	0.029	0.165	0.479	0.000
1	10	2	0.034	0.389	(30%)	0.278	0.039	0.065	0.115	0.312	0.055
1	11	2	0.031	0.179	(20%)	0.220	0.052	0.080	0.128	0.124	0.073
2	1	3	0.000	1.081	(66%)	0.251	0.032	0.004	0.037	0.231	0.000
2	2	3	0.000	0.853	(63%)	0.244	0.032	0.008	0.034	0.180	0.000
2	3	3	0.000	0.637	(56%)	0.246	0.056	0.016	0.035	0.152	0.000
2	4	2	0.000	1.020	(64%)	0.241	0.085	0.007	0.042	0.189	0.000
2	5	4	0.039	2.468	(90%)	0.120	-0.006	0.013	0.000	0.096	0.000
2	6	2	0.113	5.094	(91%)	0.096	-0.005	0.006	0.000	0.292	0.000
2	7	4	0.101	5.617	(93%)	0.079	-0.004	0.007	0.000	0.257	0.000
2	8	3	0.062	4.304	(90%)	0.107	-0.005	0.009	0.000	0.286	0.000
2	9	3	0.000	4.751	(86%)	0.073	-0.004	0.001	0.198	0.535	0.000
2	10	4	0.000	0.297	(37%)	0.339	0.036	0.025	0.035	0.070	0.000
2	11	3	0.014	0.063	(11%)	0.297	0.040	0.033	0.045	0.021	0.042

Table 3: Fe incubations for all cycles were conducted on array or on deck and measured at the final timepoint (‘sample point’) for both control and amended samples

	Deck/ array	Sampling depth (m)	Array depth (m)	Sample point (d)	bSi (µM)		POC (µM)		Chl-a (µg L^{-1})		bSi:POC (mol:mol)	
					ctrl	+ Fe	ctrl	+ Fe	ctrl	+ Fe	ctrl	+ Fe
C1D1	deck	12	n/a	3	6.22	6.02	34.81	34.95	14.38	15.47	3.71	0.18
C1D2	array	10	8	2	6.97	6.98	42.73	54.33	17.02	14.25	6.87	0.16
C1D2	array	10	12	2	4.77	4.47	26.43	20.41	no data	no data	3.88	0.18
C1D3	deck	10	n/a	3	5.19	5.27	25.44	24.45	4.75	4.36	3.13	0.20
C2D1	deck	12	n/a	3	4.52	4.52	18.45	31.87	4.33	4.19	2.46	0.25
C2D2	array	8	10	3	4.51	4.32	12.38	29.03	5.75	7.95	1.80	0.37
C2D4	deck	15	n/a	3	3.85	3.76	10.10	24.34	3.48	5.25	1.48	0.39
C3D1	deck	12	n/a	3	1.94	1.93	9.57	14.78	3.29	2.82	1.31	0.20
C3D2	array	35	30	2	0.51	0.46	4.54	3.99	0.87	1.24	0.55	0.11
C4D1	array	30	30	2	0.60	0.53	3.87	8.33	0.54	0.39	0.43	0.16
C4D2	deck	20	n/a	4	0.23	0.32	14.85	15.68	3.21	6.81	1.88	0.02

Table 4: Lateral flux of bSi determined by transect bSi concentration and ADCP velocity data. U is East, V is North and units are μmol m^{-2} s^{-1}. Filament bounds were determined by maximum shear and filament depth was determined by deriving Brunt-Vaisala Frequency to determine degree of stratification as a function of depth.

Transect	Region	Avg J_u (μmol m^{-2} s^{-1})	stdev J_u (μmol m^{-2} s^{-1})	Avg J_v (μmol m^{-2} s^{-1})	stdev J_v (μmol m^{-2} s^{-1})
1	filament	-55	82	-170	155
1	entire transect	-24	81	-103	133
2	filament	-422	272	234	266
2	entire transect	-239	251	93	220

Table 5: Export data table for sediment traps throughout cycles and drifter between C2 and C4 (R2).

		bSi export (mmol Si m^{-2} d^{-1})	POC export (mmol m^{-2} d^{-1})	bSi:POC export (mol:mol)
~ bottom of euphotic zone	C1	15.90	29.26	0.54
	C2	10.51	44.43	0.24
	C3	3.50	46.62	0.08
	C4	11.06	35.70	0.31
	R2	5.28	45.78	0.12
100 m	C1	12.60	16.95	0.74
	C2	6.21	16.50	0.38
	C3	1.50	12.83	0.12
	C4	8.34	26.68	0.31
	R2	*no data*	*no data*	*no data*
150 m	C1	13.27	19.65	0.68
	C2	5.31	15.31	0.35
	C3	0.85	6.80	0.12
	C4	6.80	25.87	0.26
	R2	2.13	14.87	0.14

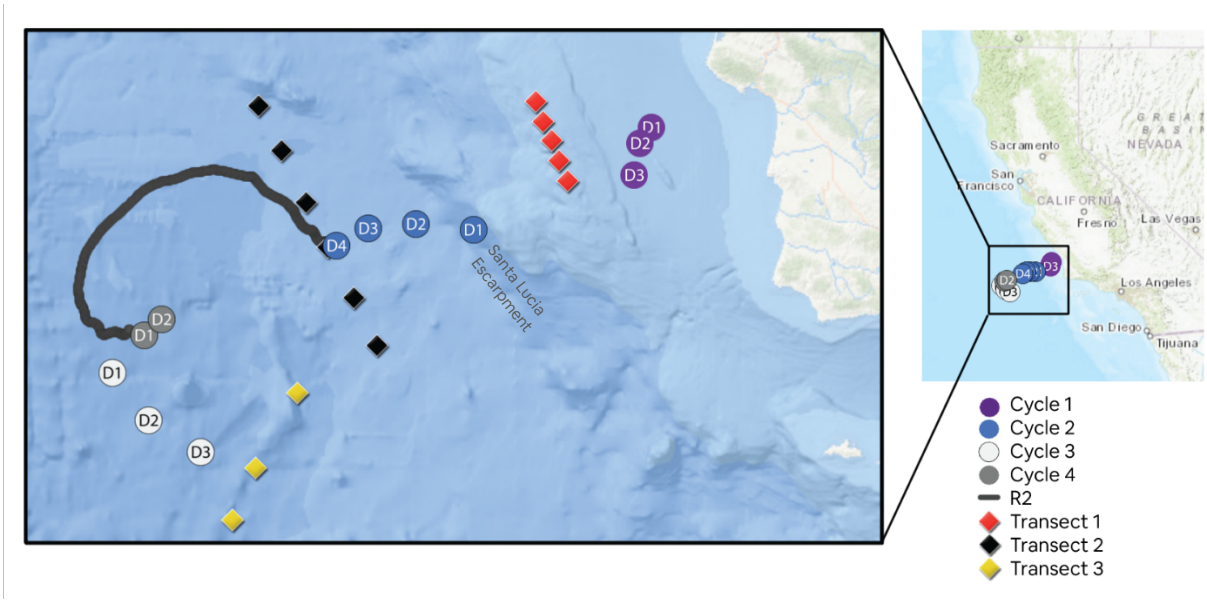

Figure 1: Map of Cycle and R2 locations, Jun 9 – Jun 25 2017

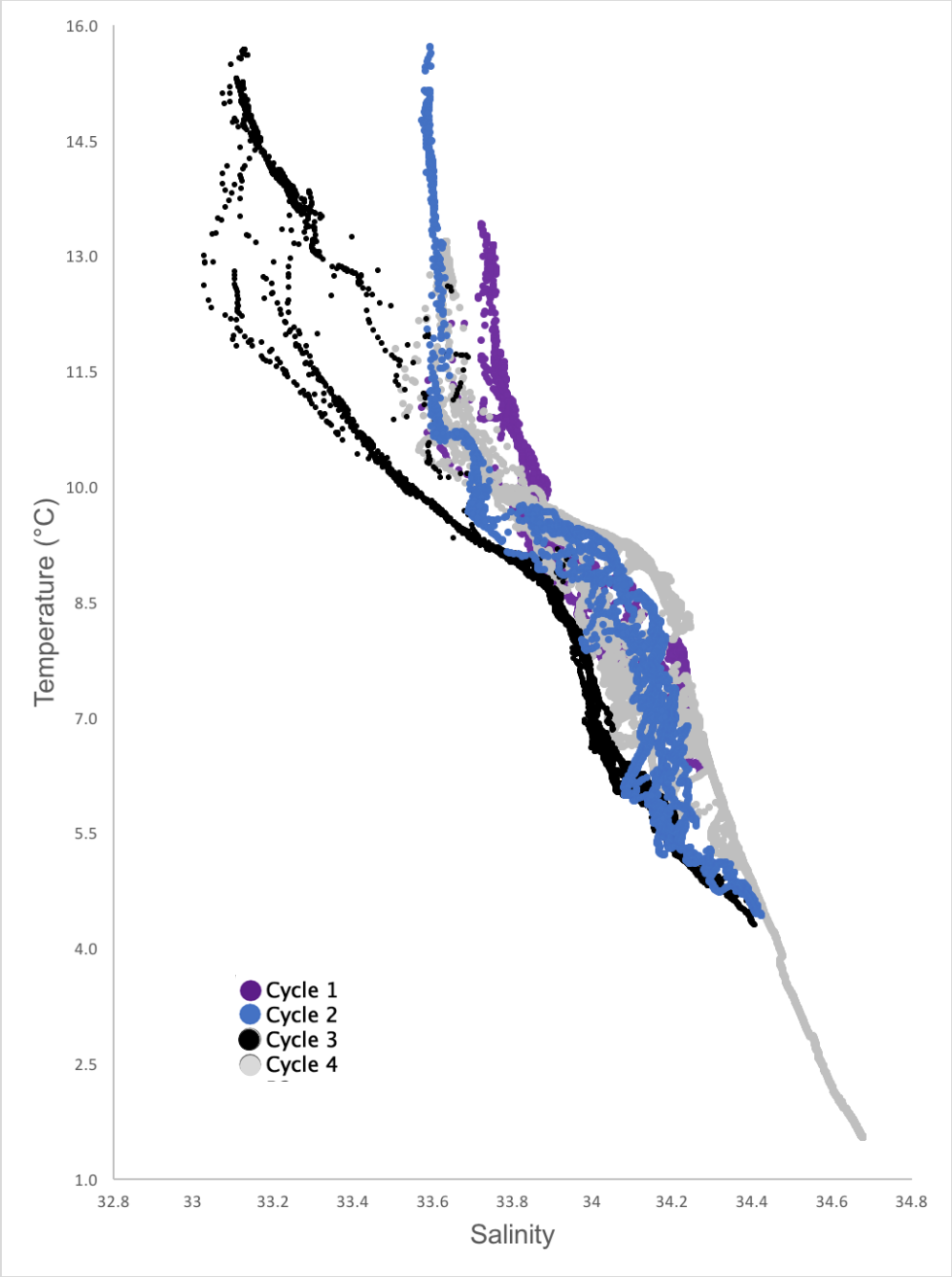

Figure 2: Temperature vs. Salinity of Cycles 1-4. Cycle 3 (black) is divergent from all other cycles, while Cycles 2 and 4 are most similar. Cycle 1 appears to be similar to Cycles 2 and 4, but slightly more saline.

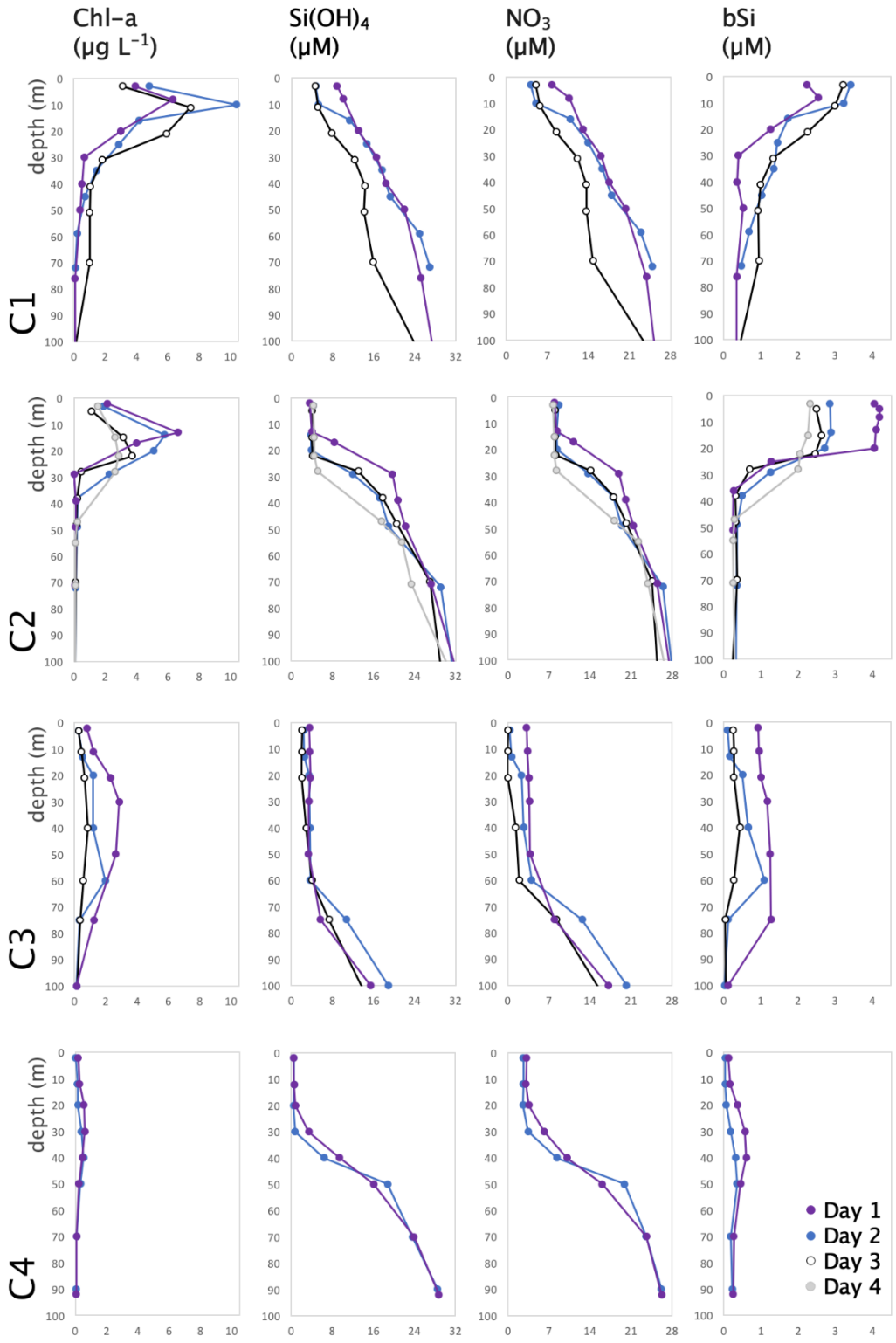

Figure 3: In situ profiles for a) chl-a b) $Si(OH)_4$ c) NO_3 and d) bSi to 100 m depth for all days of all four cycles.

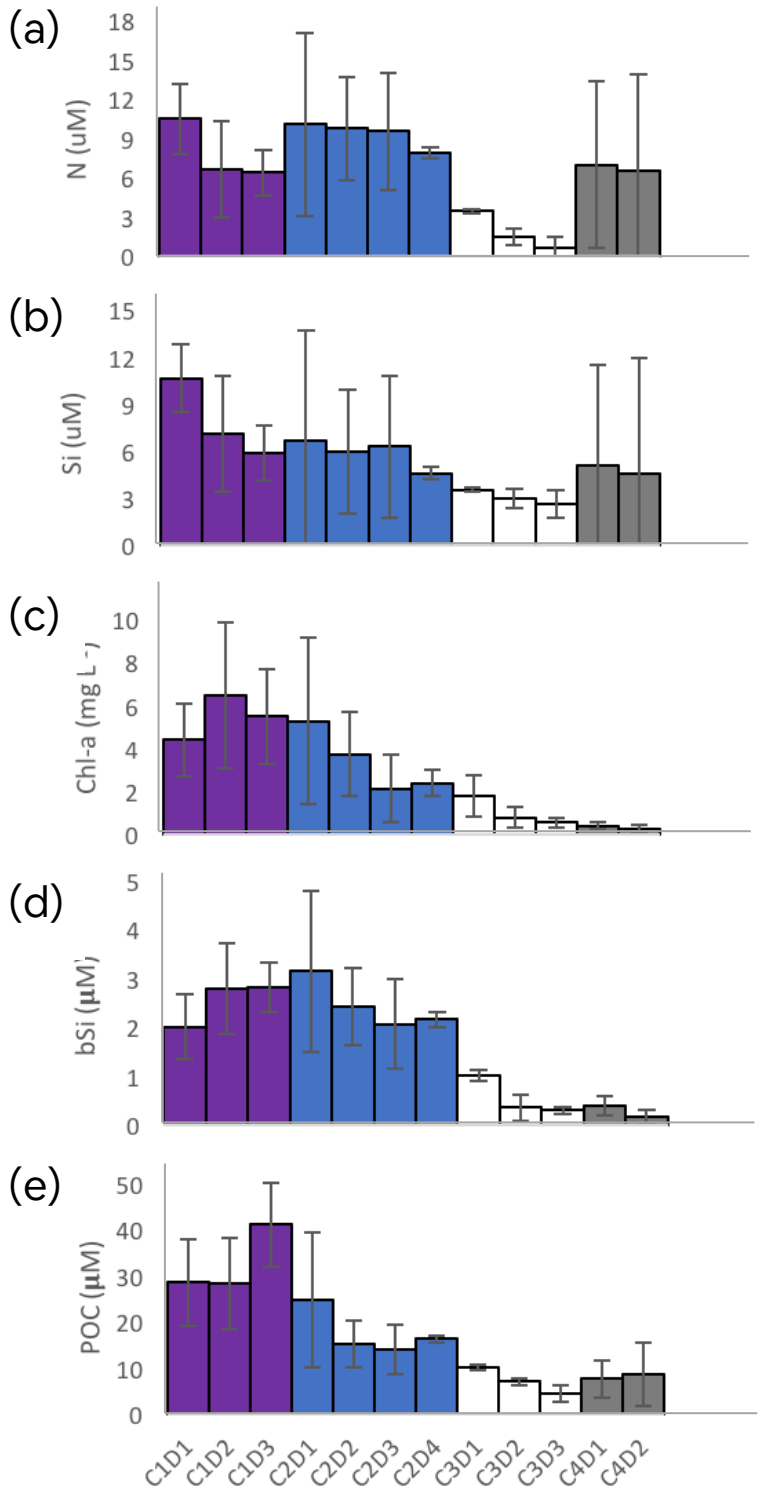

Figure 4: Trends across all cycles, vertically integrated over the euphotic zone.

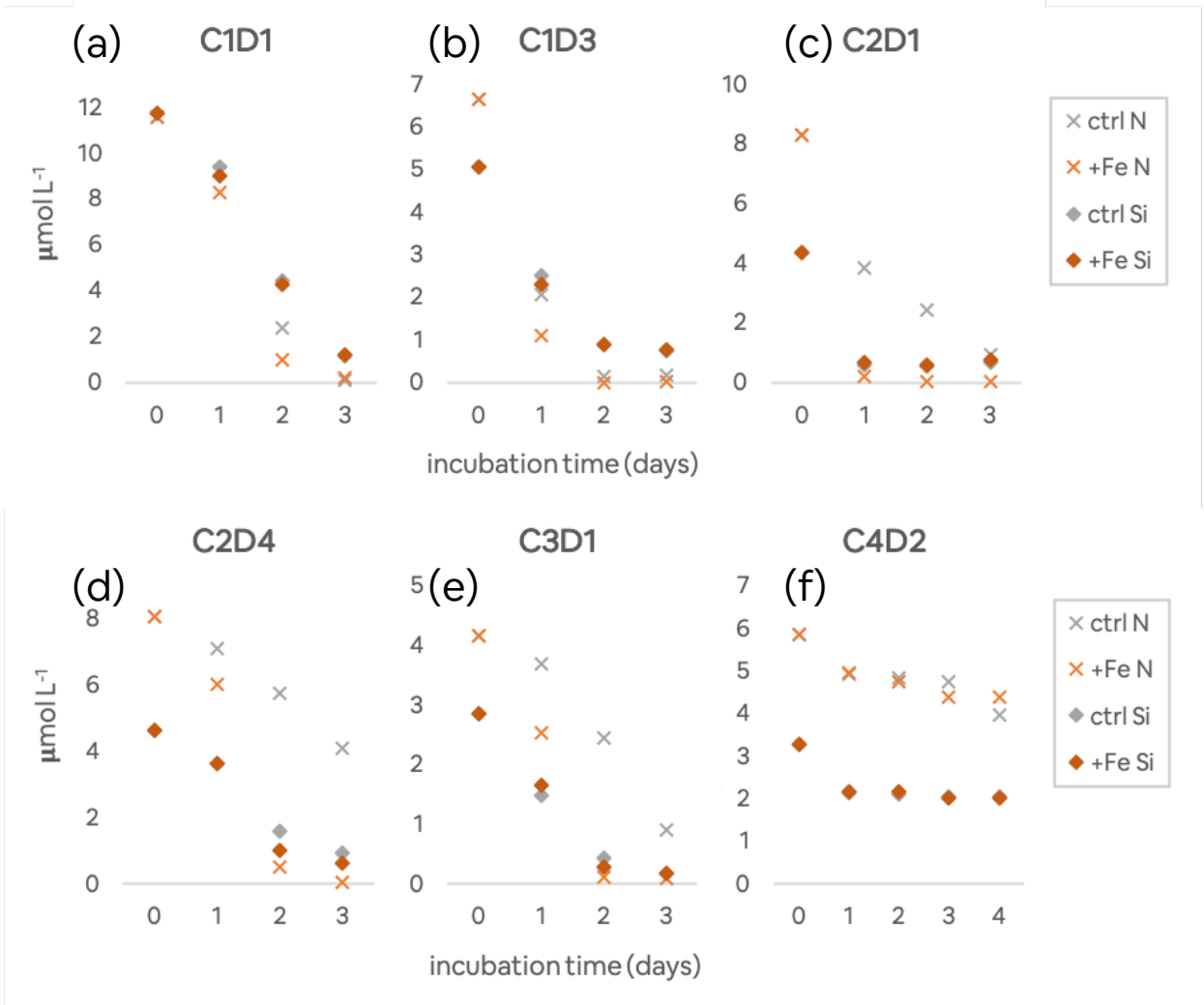

Figure 5: In situ Si and N in on-deck Fe incubation samples by day.

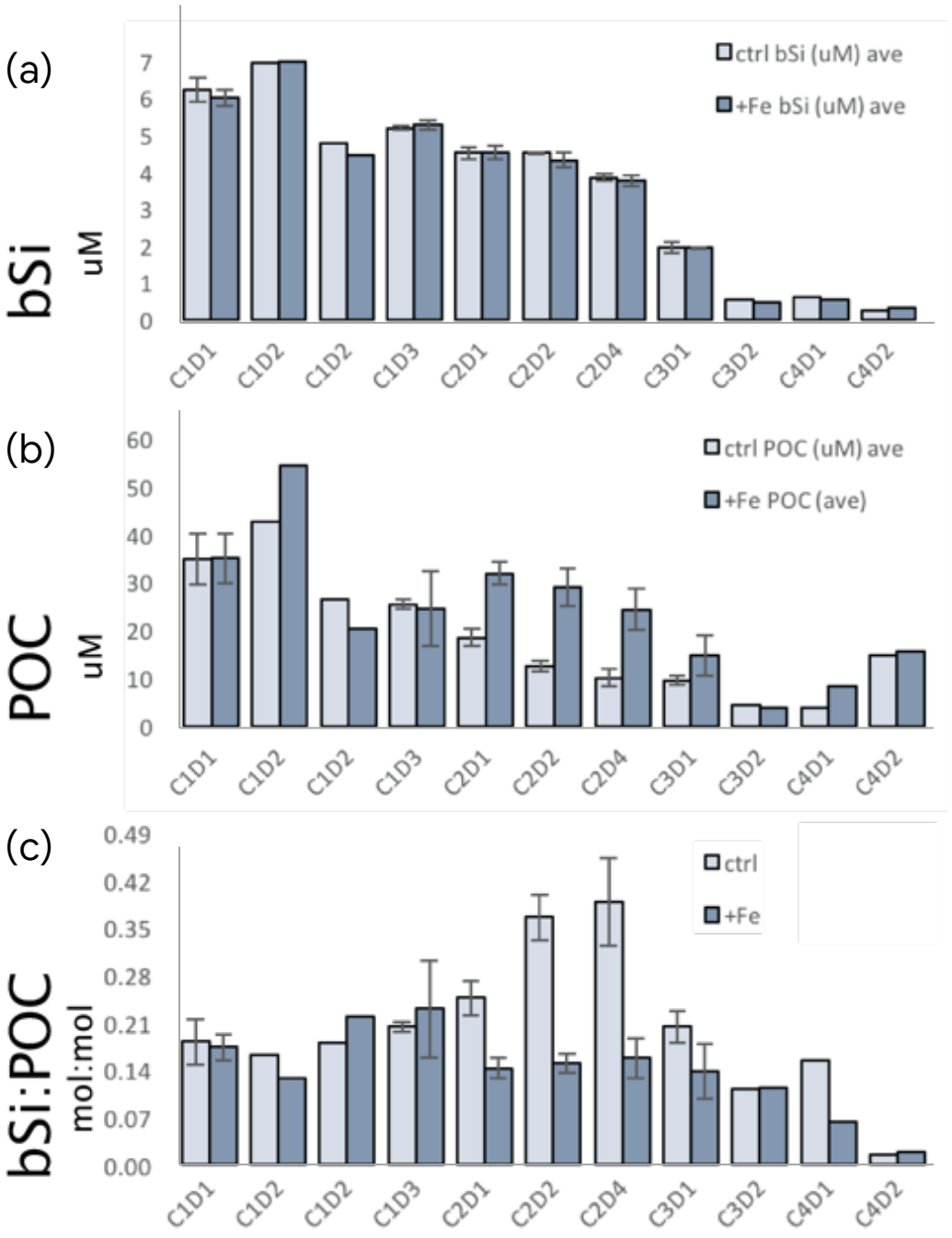

Figure 6: Fe addition grow-out experiment bSi and POC. bSi appears to be stable between control and amended experiments, while POC of previously diatom Fe limited experiments increases significantly in response to Fe amendment, resulting in a decreased bSi:POC primarily due to changes in POC.

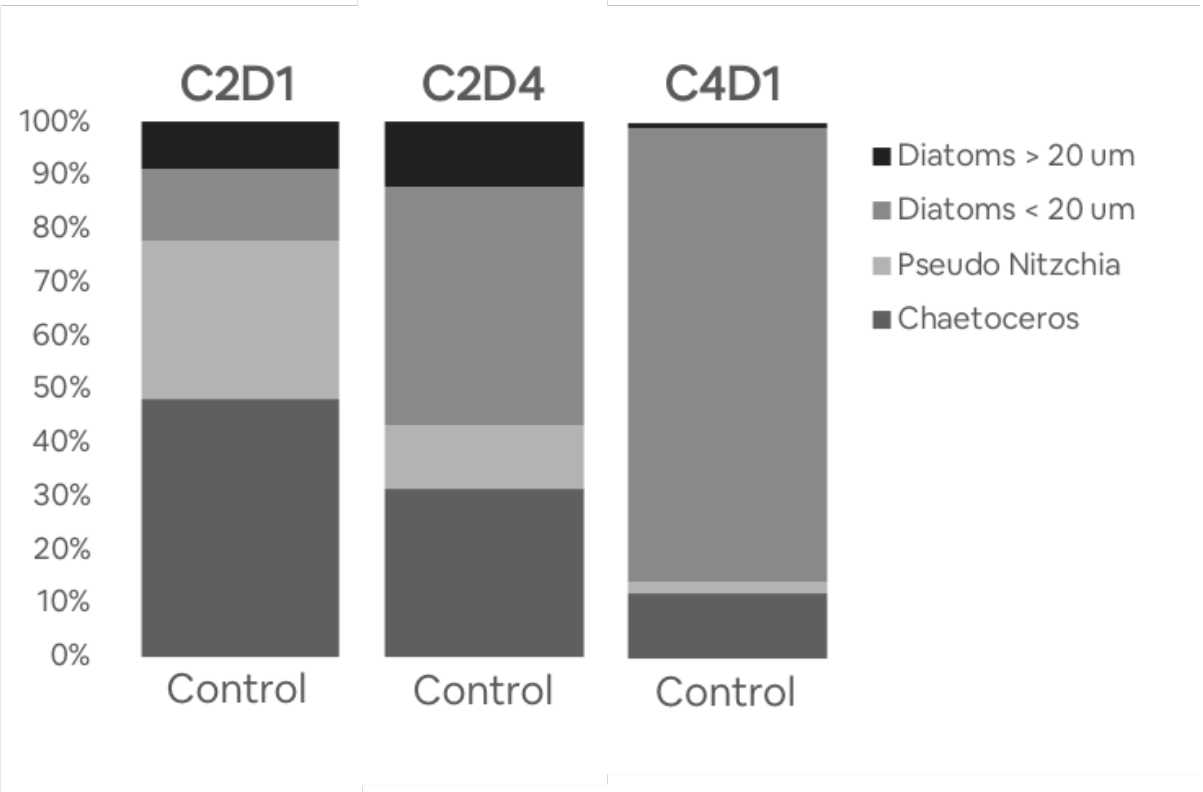

Figure 7: Diatom community composition, observed via microscopy, of control samples from incubation studies in C2 and C4. C3 was omitted because it does not appear to be a part of the filament and C1 because microscopy samples were not collected.

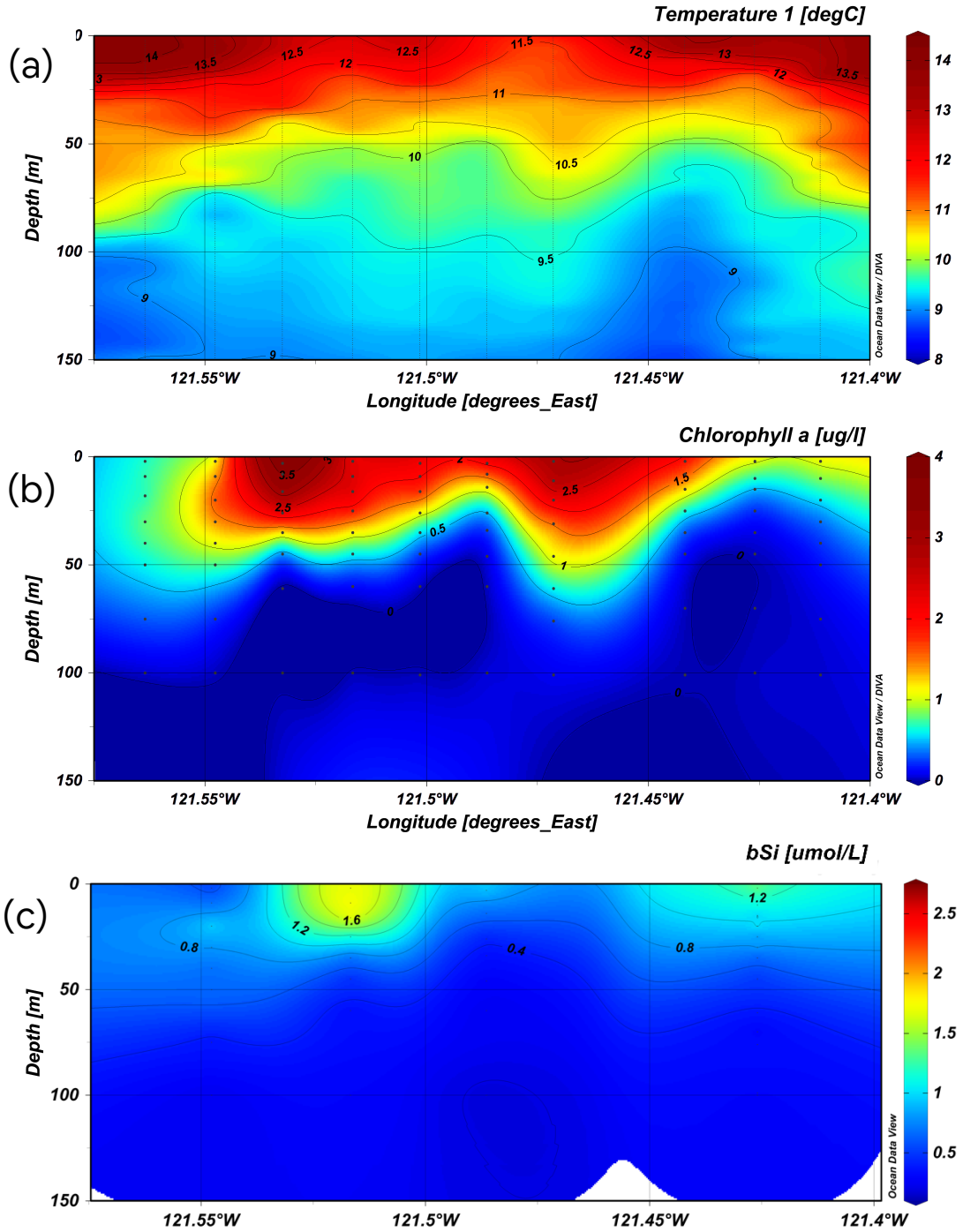

Figure 8. Section plots of Transect 1 (a) potential temperature, (b) chl-a and (c) bSi for stations 1-11. Station 8 is not shown.

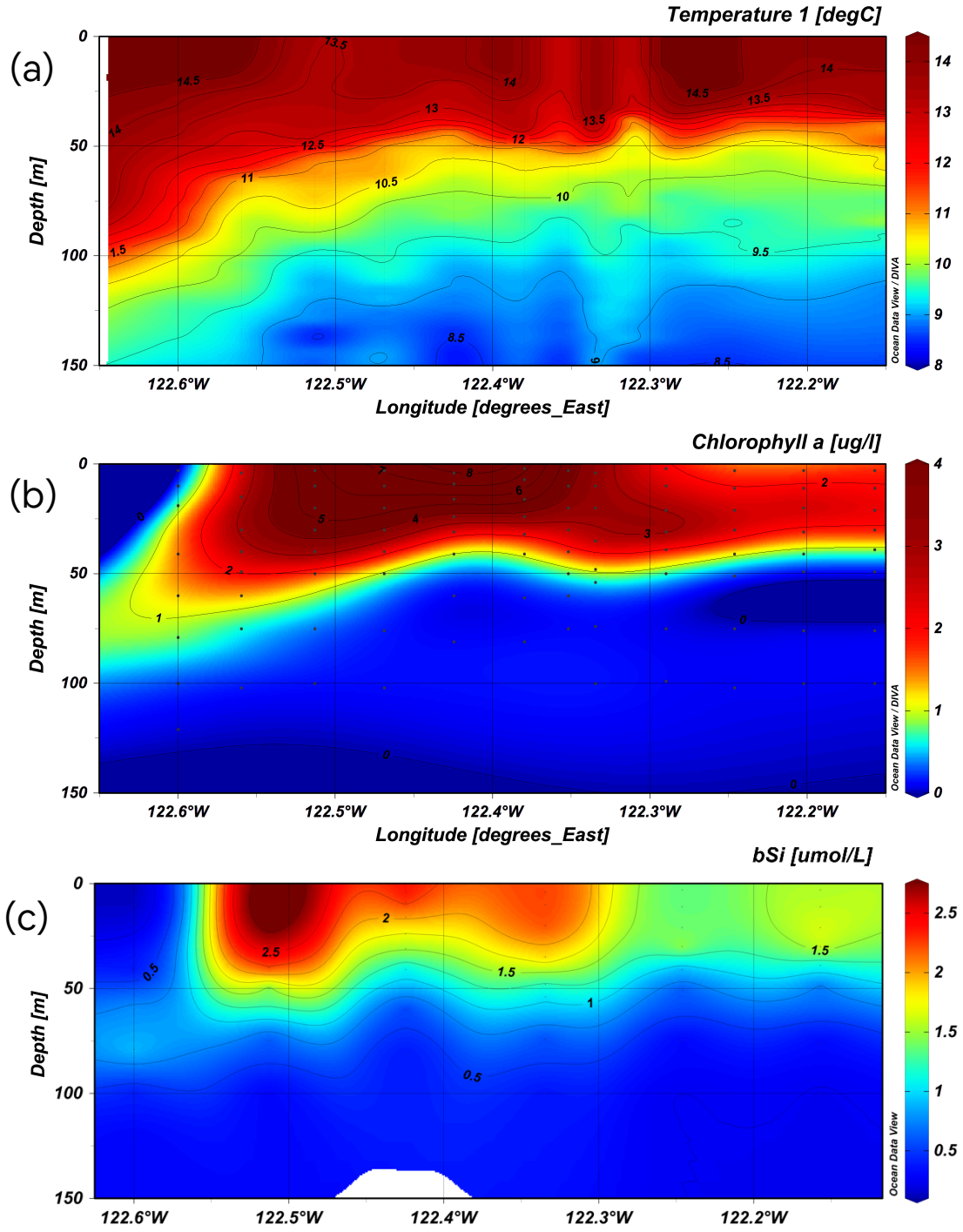

Figure 9. Section plots of Transect 2 (a) potential temperature, (b) chl-a and (c) bSi for stations 1-11.

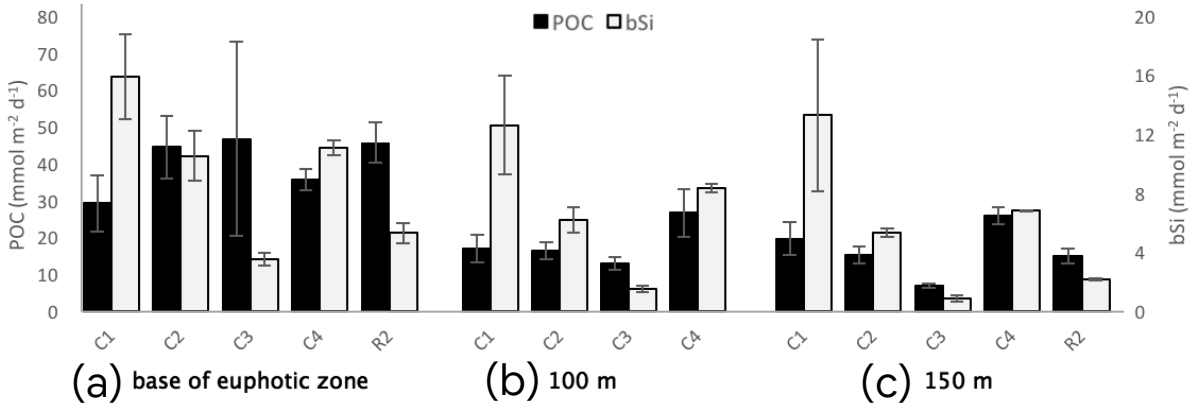

Figure 10: Trends in bSi and POC in export data

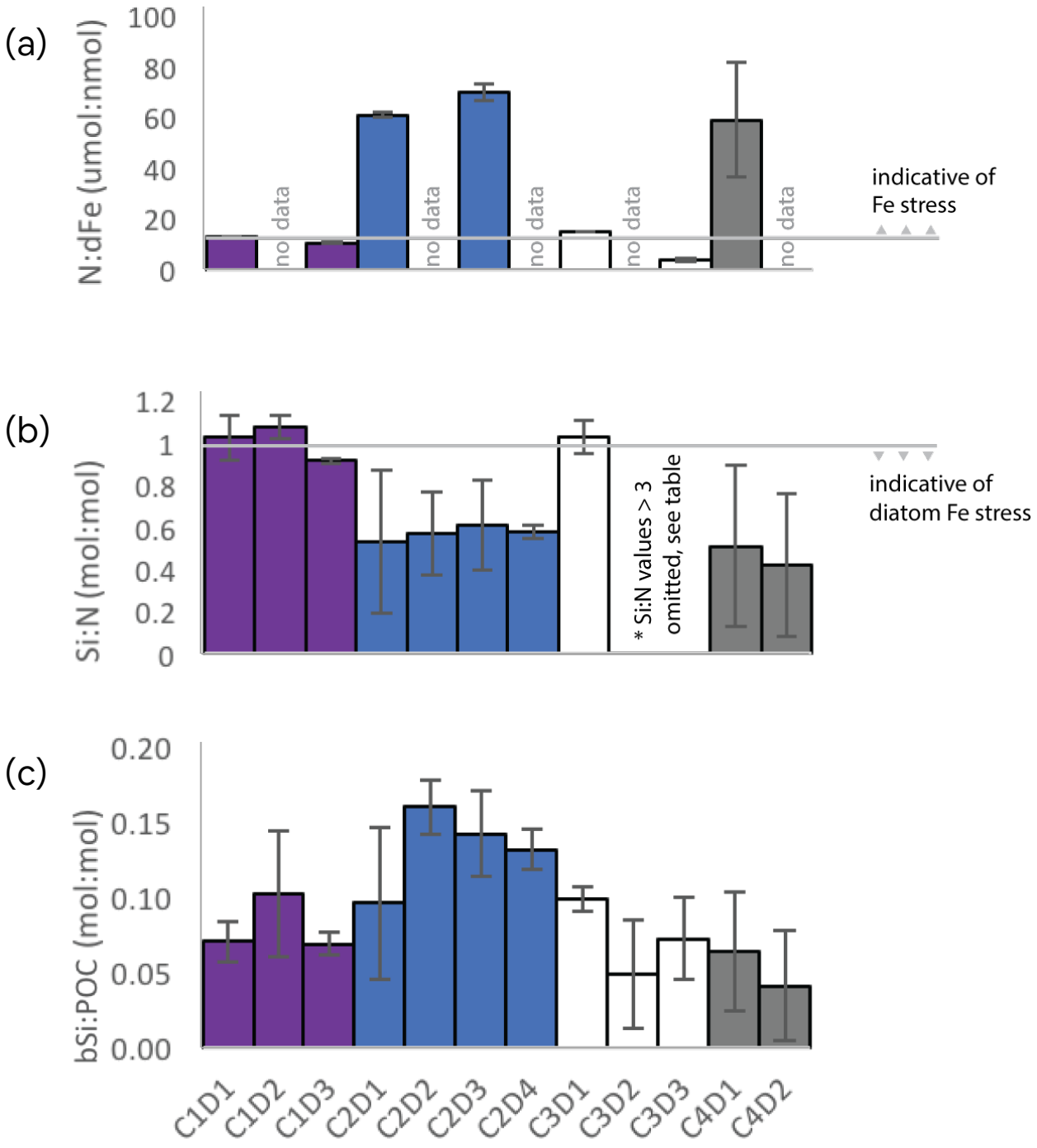

Figure 11: In situ indications of diatom Fe limitation and bSi:POC, vertically integrated over the euphotic zone.

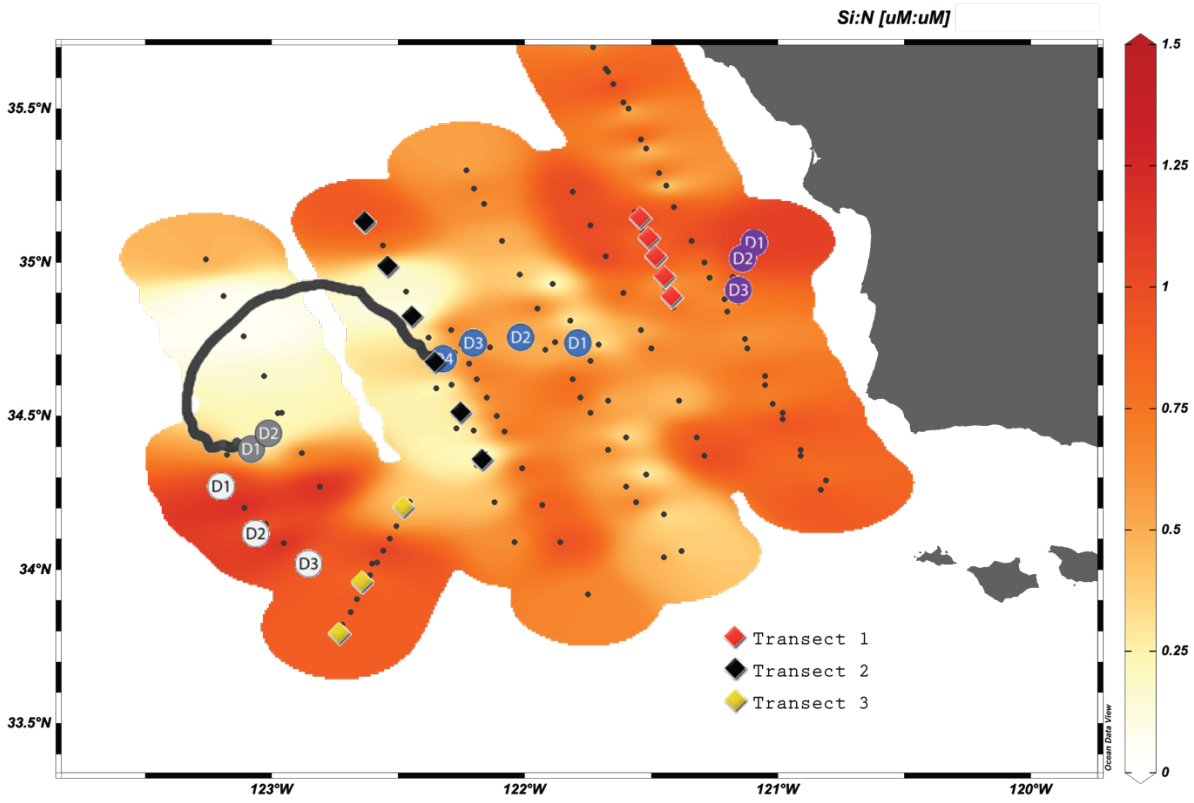

Figure 12: Cycles are marked with circles, with the day of the Cycle indicated. Transects are marked with diamonds, with the southmost points being the first station sampled. Black dots are surface data acquired from underway samples from the ship's flow-through system.

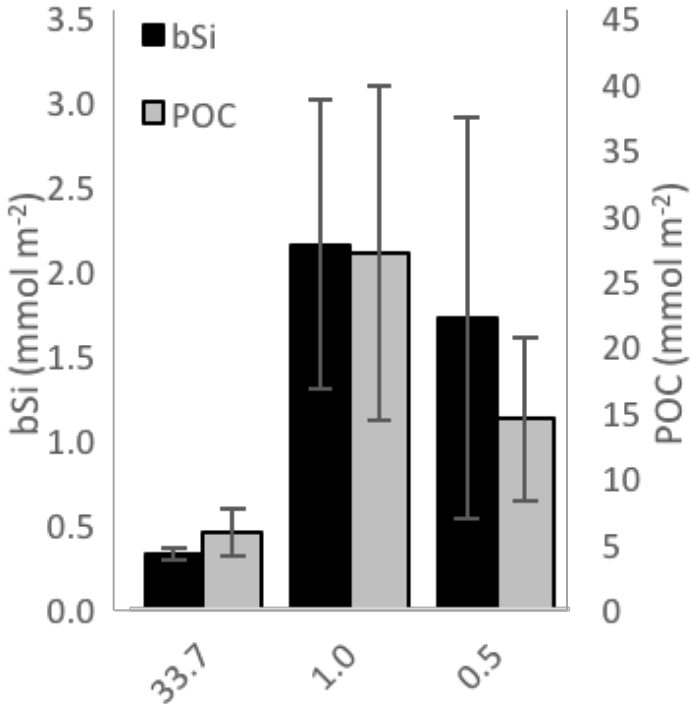

Figure 13: Patterns of average bSi and POC as a function of average Si:N vertically integrated over the euphotic zone.

This thesis is coauthored with Kiefer Forsch, Katherine A. Barbeau, Jeffrey W. Krause, Michael R. Stukel, and Ralf Goericke. The thesis author was the primary author of this material.

7. References

Assmy, P., Smetacek, V., Montresor, M., Klaas, C., Henjes, J., Strass, V. H., Arrieta, J. M., Bathmann, U., Berg, G. M., Breitbarth, E., Cisewski, B., Friedrichs, L., Fuchs, N., Herndl, G. J., Jansen, S., Kragefsky, S., Latasa, M., Peeken, I., Rottgers, R., et al. (2013). Thick-shelled, grazer-protected diatoms decouple ocean carbon and silicon cycles in the iron-limited Antarctic Circumpolar Current. *Proceedings of the National Academy of Sciences*, *110*(51), 20633–20638. https://doi.org/10.1073/pnas.1309345110

Barth, J. A., & Brink, K. H. (1987). Shipboard acoustic doppler profiler velocity observations near point conception' spring 1983. *Journal of Geophysical Research: Oceans*. https://doi.org/10.1029/JC092iC04p03925

Biller, D. V., Coale, T. H., Till, R. C., Smith, G. J., & Bruland, K. W. (2013). Coastal iron and nitrate distributions during the spring and summer upwelling season in the central California Current upwelling regime. *Continental Shelf Research*. https://doi.org/10.1016/j.csr.2013.07.003

Boyle, E. (1998). Pumping iron makes thinner diatoms. *Natural Hazards*, *393*(6687), 2–3. https://doi.org/10.1038/31585

Bruland, K. W., Rue, E. L., & Smith, G. J. (2001). Iron and macronutrients in California coastal upwelling regimes: Implications for diatom blooms. *Limnol. Oceanogr*, *46*(7), 1661–1674. https://doi.org/10.4319/lo.2001.46.7.1661

Bruland, K. W., Rue, E. L., Smith, G. J., & DiTullio, G. R. (2005). Iron, macronutrients and diatom blooms in the Peru upwelling regime: Brown and blue waters of Peru. *Marine Chemistry*, *93*(2–4), 81–103. https://doi.org/10.1016/j.marchem.2004.06.011

Brzezinski, M. A. (1985). The Si:C:N Ratio of Marine Diatoms: Interspecific Variability and the Effect of Some Environmental Variables. *Journal of Phycology*, *21*(3), 347–357. https://doi.org/10.1111/j.0022-3646.1985.00347.x

Brzezinski, M. A., & Nelson, D. M. (1995). The annual silica cycle in the Sargasso Sea near Bermuda. *Deep-Sea Research Part I*, *42*(7), 1215–1237. https://doi.org/10.1016/0967-0637(95)93592-3

Brzezinski, M. A., Krause, J. W., Bundy, R. M., Barbeau, K. A., Franks, P., Goericke, R., Landry, M. R., & Stukel, M. R. (2015). Enhanced silica ballasting from iron stress sustains carbon export in a frontal zone within the California Current. *Journal of Geophysical Research: Oceans*, *120*(7), 4654–4669. https://doi.org/10.1002/2015JC010829.Received

Bundy, R. M., Jiang, M., Carter, M., & Barbeau, K. A. (2016). Iron-Binding Ligands in the Southern California Current System: Mechanistic Studies. *Frontiers in Marine Science*, *3*(March), 1–17. https://doi.org/10.3389/fmars.2016.00027

Carr, M. E. (2002). Estimation of potential productivity in Eastern Boundary Currents using

remote sensing. *Deep-Sea Research Part II: Topical Studies in Oceanography*, *49*(1–3), 59–80. https://doi.org/10.1016/S0967-0645(01)00094-7

Carr, M. E., & Kearns, E. J. (2003). Production regimes in four Eastern Boundary Current systems. *Deep-Sea Research Part II: Topical Studies in Oceanography*, *50*(22–26), 3199–3221. https://doi.org/10.1016/j.dsr2.2003.07.015

Centurioni, L. R., Ohlmann, J. C., & Niiler, P. P. (2008). Permanent Meanders in the California Current System. *Journal of Physical Oceanography*. https://doi.org/10.1175/2008jpo3746.1

Chase, Z., Strutton, P. G., & Hales, B. (2007). Iron links river runoff and shelf width to phytoplankton biomass along the U.S. West Coast. *Geophysical Research Letters*, *34*(4), 10–13. https://doi.org/10.1029/2006GL028069

Checkley, D. M., & Barth, J. A. (2009). Patterns and processes in the California Current System. *Progress in Oceanography*, *83*(1–4), 49–64. https://doi.org/10.1016/j.pocean.2009.07.028

Drake, P. T., Edwards, C. A., & Barth, J. A. (2011). Dispersion and connectivity estimates along the U.S. west coast from a realistic numerical model. *Journal of Marine Research*. https://doi.org/10.1357/002224011798147615

Field, C. B., Behrenfeld, M. J., Randerson, J. T., & Falkowski, P. G. (1998). Primary Production of the Biosphere: Integrating Terrestrial and Oceanic Components. *Science*, *281*(5374), 237–240. https://doi.org/10.1126/science.281.5374.237

Firme, G. F., Rue, E. L., Weeks, D. A., Bruland, K. W., & Hutchins, D. A. (2003). Spatial and temporal variability in phytoplankton iron limitation along the California coast and consequences for Si, N, and C biogeochemistry. *Global Biogeochemical Cycles*, *17*(1), 1–13. https://doi.org/10.1029/2001GB001824

Franck, V. M., Brzezinski, M. A., Coale, K. H., & Nelson, D. M. (2000). Iron and silicic acid concentrations regulate Si uptake north and south of the Polar Frontal Zone in the Pacific Sector of the Southern Ocean. *Deep-Sea Research Part II: Topical Studies in Oceanography*, *47*(15–16), 3315–3338. https://doi.org/10.1016/S0967-0645(00)00070-9

Franck, V. M., Bruland, K. W., Hutchins, D. A., & Brzezinski, M. A. (2003). Iron and zinc effects on silicic acid and nitrate uptake kinetics in three high-nutrient, low-chlorophyll (HNLC) regions. *Marine Ecology Progress Series*, *252*(3), 15–33. https://doi.org/10.3354/meps252015

Goericke, R. (2011). The structure of marine phytoplankton communities- patterns, rules and mechanisms. *California Cooperative Oceanic Fisheries Investigations Reports*, *52*, 182–197.

Goericke, R., & Montoya, J. P. (1998). Estimating the contribution of microalgal taxa to chlorophyll a in the field - Variations of pigment ratios under nutrient- and light-limited growth. *Marine Ecology Progress Series*, *169*, 97–112. https://doi.org/10.3354/meps169097

Hoffmann, L. J., Peeken, I., & Lochte, K. (2007). Effects of iron on the elemental stoichiometry during EIFEX and in the diatoms Fragilariopsis kerguelensis and Chaetoceros dichaeta. *Biogeosciences*, *4*(4), 569–579. https://doi.org/10.5194/bg-4-569-2007

Homoky, W. B., Severmann, S., McManus, J., Berelson, W. M., Riedel, T. E., Statham, P. J., & Mills, R. A. (2012). Dissolved oxygen and suspended particles regulate the benthic flux of iron from continental margins. *Marine Chemistry*. https://doi.org/10.1016/j.marchem.2012.03.003

Hösen, E., Möller, J., Jochumsen, K., & Quadfasel, D. (2016). Scales and properties of cold filaments in the Benguela upwelling system off Lüderitz. *Journal of Geophysical Research: Oceans*, *121*(3), 1896–1913. https://doi.org/10.1002/2015JC011411

Hutchins, D. A., & Bruland, K. W. (1998). Iron-limited diatom growth and Si : N uptake ratios in a coastal upwelling regime. *Nature*, *393*(June), 561–564. https://doi.org/Doi 10.1038/31203

Hutchins, D. A., DiTullio, G. R., Zhang, Y., & Bruland, K. W. (1998). An iron limitation mosaic in the California upwelling regime. *Limnology and Oceanography*, *43*(6), 1037–1054. https://doi.org/10.4319/lo.1998.43.6.1037

Hutchins, D. A., Alm, B., Riseman, S. F., Maucher, J. M., Geesey, M. E., Trick, C. G., Smith, G. J., Rue, E. L., Bruland, K. W., Hare, C. E., Weaver, R. S., Zhang, Y., & Firme, G. F. (2002). Phytoplankton iron limitation in the Humboldt Current and Peru Upwelling. *Limnology*, *47*(4), 997–1011.

Johnson, K. S., Chavez, F. P., & Friederich, G. E. (1999). Continental-shelf sediment as a primary source of iron for coastal phytoplankton. *Nature*, *398*(6729), 697–700. https://doi.org/10.1038/19511

Karlson, B., Cusack, C., & Bresnan, E. (2010). Microscopic and Molecular Methods for Quantitative Phytoplankton Analysis. *Exchange Organizational Behavior Teaching Journal*, *1037*(3), 110. Retrieved from http://www.ncbi.nlm.nih.gov/pubmed/21262932

Kelly, T. B., Goericke, R., Kahru, M., Song, H., & Stukel, M. R. (2018). CCE II: Spatial and interannual variability in export efficiency and the biological pump in an eastern boundary current upwelling system with substantial lateral advection. *Deep Sea Research Part I: Oceanographic Research Papers*, *140*(August), 14–25. https://doi.org/10.1016/j.dsr.2018.08.007

Kim, S. Y., Terrill, E. J., Cornuelle, B. D., Jones, B., Washburn, L., Moline, M. A., Paduan, J. D., Garfield, N., Largier, J. L., Crawford, G., & Kosro, P. M. (2011). Mapping the U.S. West Coast surface circulation: A multiyear analysis of high-frequency radar observations. *Journal of Geophysical Research: Oceans*. https://doi.org/10.1029/2010JC006669

King, A. L., & Barbeau, K. A. (2007). Evidence for phytoplankton iron limitation in the southern California Current System. *Marine Ecology Progress Series*, *342*, 91–103. https://doi.org/10.3354/meps342091

King, A. L., & Barbeau, K. A. (2011). Dissolved iron and macronutrient distributions in the southern California Current System. *Journal of Geophysical Research: Oceans*, *116*(3), C03018. https://doi.org/10.1029/2010JC006324

King, A. L., Buck, K. N., & Barbeau, K. A. (2012). Quasi-Lagrangian drifter studies of iron speciation and cycling off Point Conception, California. *Marine Chemistry*, *128–129*, 1–12. https://doi.org/10.1016/j.marchem.2011.11.001

Knauer, G. A., Martin, J. H., & Bruland, K. W. (1979). Fluxes of particulate carbon, nitrogen, and phosphorus in the upper water column of the northeast Pacific. *Deep Sea Research Part A, Oceanographic Research Papers*, *26*(1), 97–108. https://doi.org/10.1016/0198-0149(79)90089-X

Krause, J. W., Brzezinski, M. A., Goericke, R., Landry, M. R., Ohman, M. D., Stukel, M. R., & Taylor, A. G. (2015). Variability in diatom contributions to biomass, organic matter production and export across a frontal gradient in the California Current Ecosystem. *Journal of Geophysical Research: Oceans*, *120*(2), 1032–1047. https://doi.org/10.1002/2014JC010472

De La Rocha, C. L., Hutchins, D. A., Brzezinski, M. A., & Zhang, Y. (2000). Effects of iron and zinc deficiency on elemental composition and silica production by diatoms. *Marine Ecology Progress Series*, *195*, 71–79. https://doi.org/10.3354/meps195071

Landry, M. R., Ohman, M. D., Goericke, R., Stukel, M. R., & Tsyrklevich, K. (2009). Lagrangian studies of phytoplankton growth and grazing relationships in a coastal upwelling ecosystem off Southern California. *Progress in Oceanography*, *83*(1–4), 208–216. https://doi.org/10.1016/j.pocean.2009.07.026

Leblanc, K., Hare, C. E., Boyd, P. W., Bruland, K. W., Sohst, B., Pickmere, S., Lohan, M. C., Buck, K., Ellwood, M., & Hutchins, D. A. (2005). Fe and Zn effects on the Si cycle and diatom community structure in two contrasting high and low-silicate HNLC areas. *Deep-Sea Research Part I: Oceanographic Research Papers*, *52*(10), 1842–1864. https://doi.org/10.1016/j.dsr.2005.06.005

Leynaert, a., Bucciarelli, E., Claquin, P., Dugdale, R. C., Martin-Jézéquel, V., Pondaven, P., & Ragueneau, O. (2004). Effect of iron deficiency on diatom cell size and silicic acid uptake kinetics. *Limnology and Oceanography*, *49*(4), 1134–1143. https://doi.org/10.4319/lo.2004.49.4.1134

Li, Q. P., Franks, P. J. S., Landry, M. R., Goericke, R., & Taylor, A. G. (2010). Modeling phytoplankton growth rates and chlorophyll to carbon ratios in California coastal and pelagic ecosystems. *Journal of Geophysical Research: Biogeosciences*, *115*(4), 1–12. https://doi.org/10.1029/2009JG001111

Lohan, M. C., Aguilar-islas, A. M., & Bruland, K. W. (2006). OCEANOGRAPHY : METHODS Direct determination of iron in acidified (pH 1 . 7) seawater samples by flow injection analysis with catalytic spectrophotometric detection : Application and intercomparison, 164–171.

Marchetti, A., & Cassar, N. (2009). Diatom elemental and morphological changes in response to iron limitation: A brief review with potential paleoceanographic applications. *Geobiology*, *7*(4), 419–431. https://doi.org/10.1111/j.1472-4669.2009.00207.x

Marchetti, A., & Harrison, P. J. (2007). Coupled changes in the cell morphology and elemental (C, N, and Si) composition of the pennate diatom Pseudo-nitzschia due to iron deficiency. *Limnology and Oceanography*, *52*(5), 2270–2284. https://doi.org/10.4319/lo.2007.52.5.2270

Martin-Jézéquel, V., Hildebrand, M., & Brzezinski, M. A. (2000). Silicon metabolism in diatoms: Implications for growth. *Journal of Phycology*, *36*(5), 821–840. https://doi.org/10.1046/j.1529-8817.2000.00019.x

Mohrholz, V., Eggert, A., Junker, T., Nausch, G., Ohde, T., & Schmidt, M. (2014). Cross shelf hydrographic and hydrochemical conditions and their short term variability at the northern Benguela during a normal upwelling season. *Journal of Marine Systems*. https://doi.org/10.1016/j.jmarsys.2014.04.019

Moore, J. K., Doney, S. C., Glover, D. M., & Fung, I. Y. (2002). Iron cycling and nutrient limitation patterns in surface waters of the world ocean. *Deep-Sea Research Part II - Topical Studies in Oceanography*, *49*, 463–507.

Morrow, R. M., Ohman, M. D., Goericke, R., Kelly, T. B., Stephens, B. M., & Stukel, M. R. (2018). CCE V: Primary production, mesozooplankton grazing, and the biological pump in the California Current Ecosystem: Variability and response to El Niño. *Deep-Sea Research Part I: Oceanographic Research Papers*, *140*(January), 52–62. https://doi.org/10.1016/j.dsr.2018.07.012

Muller, A. A., Mohrholz, V., & Schmidt, M. (2013). The circulation dynamics associated with a northern Benguela upwelling filament during October 2010. *Continental Shelf Research*. https://doi.org/10.1016/j.csr.2013.04.037

Nagai, T., Gruber, N., Frenzel, H., Lachkar, Z., McWilliams, J. C., & Plattner, G. K. (2015). Dominant role of eddies and filaments in the offshore transport of carbon and nutrients in the California Current System. *Journal of Geophysical Research: Oceans*. https://doi.org/10.1002/2015JC010889

Nelson, D. M., Tréguer, P., Brzezinski, M. A., Leynaert, A., & Quéguiner, B. (1995). Production and dissolution of biogenic silica in the ocean: Revised global estimates, comparison with regional data and relationship to biogenic sedimentation. *Global Biogeochemical Cycles*, *9*(3), 359–372. https://doi.org/10.1029/95GB01070

Van Oostende, N., Dunne, J. P., Fawcett, S. E., & Ward, B. B. (2015). Phytoplankton succession explains size-partitioning of new production following upwelling-induced blooms. *Journal of Marine Systems*, *148*, 14–25. https://doi.org/10.1016/j.jmarsys.2015.01.009

Paasche, E. (1973). Silicon and the ecology of marine plankton diatoms. I. Thalassiosira pseudonana (Cyclotella nana) grown in a chemostat with silicate as limiting nutrient.

Marine Biology, *19*(2), 117–126. https://doi.org/10.1007/BF00353582

Plattner, G. K., Gruber, N., Frenzel, H., & McWilliams, J. C. (2005). Decoupling marine export production from new production. *Geophysical Research Letters*, *32*(11), 1–4. https://doi.org/10.1029/2005GL022660

Price, N. M. (2005). The elemental stoichiometry and composition of an iron-limited diatom. *Limnology and Oceanography*, *50*(4), 1159–1171. https://doi.org/10.4319/lo.2005.50.4.1159

Quéguiner, B. (2013). Iron fertilization and the structure of planktonic communities in high nutrient regions of the Southern Ocean. *Deep-Sea Research Part II: Topical Studies in Oceanography*, *90*, 43–54. https://doi.org/10.1016/j.dsr2.2012.07.024

Rossi, V., Garçon, V., Tassel, J., Romagnan, J. B., Stemmann, L., Jourdin, F., Morin, P., & Morel, Y. (2013). Cross-shelf variability in the Iberian Peninsula Upwelling System: Impact of a mesoscale filament. *Continental Shelf Research*. https://doi.org/10.1016/j.csr.2013.04.008

Sangrà, P., Troupin, C., Barreiro-González, B., Desmond Barton, E., Orbi, A., & Arístegui, J. (2015). The Cape Ghir filament system in August 2009 (NW Africa). *Journal of Geophysical Research C: Oceans*. https://doi.org/10.1002/2014JC010514

Sedwick, P. N., Ditullio, R., & Mackey, D. J. (2000). Iron and manganese in the Ross Sea, Antarctica: *Journal of Geophysical Research*, *105*(C5), 11,321-11,336.

Smetacek, V. (1999). Diatoms and the Ocean Carbon Cycle. *Protist*, *150*(1), 25–32. https://doi.org/10.1016/S1434-4610(99)70006-4

Smith, S. R., Gillard, J. T. F., Kustka, A. B., McCrow, J. P., Badger, J. H., Zheng, H., New, A. M., Dupont, C. L., Obata, T., Fernie, A. R., & Allen, A. E. (2016). Transcriptional Orchestration of the Global Cellular Response of a Model Pennate Diatom to Diel Light Cycling under Iron Limitation. *PLoS Genetics*, *12*(12), 1–39. https://doi.org/10.1371/journal.pgen.1006490

Stevens, I., & Johnson, J. (2003). A numerical modelling study of upwelling filaments off the NW African coast. *Oceanologica Acta*. https://doi.org/10.1016/S0399-1784(03)00049-5

Strickland, J. D. H., & Parsons, T. R. (1977). A Practical Handbook of Seawater Analysis.

Stukel, M. R., Aluwihare, L. I., Barbeau, K. A., Chekalyuk, A. M., Goericke, R., Miller, A. J., Ohman, M. D., Ruacho, A., Song, H., Stephens, B. M., & Landry, M. R. (2017). Mesoscale ocean fronts enhance carbon export due to gravitational sinking and subduction. *Proceedings of the National Academy of Sciences of the United States of America*, *114*(6), 1252–1257. https://doi.org/10.1073/pnas.1609435114

Takeda, S. (1998). Influence of iron availability on nutrient consumption ratio of diatoms in oceanic waters. *Nature*, *393*(6687), 774–777. https://doi.org/10.1038/31674

Till, C. P., Solomon, J. R., Cohen, N. R., Lampe, R. H., Marchetti, A., Coale, T. H., & Bruland, K. W. (2019). The iron limitation mosaic in the California Current System: Factors governing Fe availability in the shelf/near-shelf region. *Limnology and Oceanography*, *64*(1), 109–123. https://doi.org/10.1002/lno.11022

Timmermans, K. R., Van Der Wagt, B., & De Baar, H. J. W. (2004). Growth rates, half-saturation constants, and silicate, nitrate, and phosphate depletion in relation to iron availability of four large, open-ocean diatoms from the Southern Ocean. *Limnology and Oceanography*, *49*(6), 2141–2151. https://doi.org/10.4319/lo.2004.49.6.2141

Tréguer, P., Bowler, C., Moriceau, B., Dutkiewicz, S., Gehlen, M., Aumont, O., Bittner, L., Dugdale, R., Finkel, Z., Iudicone, D., Jahn, O., Guidi, L., Lasbleiz, M., Leblanc, K., Levy, M., & Pondaven, P. (2018). Influence of diatom diversity on the ocean biological carbon pump. *Nature Geoscience*, *11*(1), 27–37. https://doi.org/10.1038/s41561-017-0028-x

Twining, B. S., Baines, S. B., & Fisher, N. S. (2004). Element stoichiometries of individual plankton cells collected during the Southern Ocean Iron Experiment (SOFeX). *Limnology and Oceanography*, *49*(6), 2115–2128. https://doi.org/10.4319/lo.2004.49.6.2115

Wilken, S., Hoffmann, B., Hersch, N., Kirchgessner, N., Dieluweit, S., Rubner, W., Hoffmann, L. J., Merkel, R., & Peeken, I. (2011). Diatom frustules show increased mechanical strength and altered valve morphology under iron limitation. *Limnology and Oceanography*, *56*(4), 1399–1410. https://doi.org/10.4319/lo.2011.56.4.1399

Winant, C. D., Dever, E. P., & Hendershott, M. C. (2003). Characteristic patterns of shelf circulation at the boundary between central and southern California. *Journal of Geophysical Research: Oceans*. https://doi.org/10.1029/2001jc001302

Winant, C. D., Alden, D. J., Dever, E. P., Edwards, K. A., & Hendershott, M. C. (2003). Near-surface trajectories off central and southern California. *Journal of Geophysical Research: Oceans*. https://doi.org/10.1029/1999jc900083

Zentara, S. J., & Kamykowski, D. (1977). Latitudinal relationships among temperature and selected plant nutrients along the west coast of North and South America. *Journal of Marine Research*, *35*(April), 321–337.

Zhang, S., Liu, H., Ke, Y., & Li, B. (2017). Effect of the Silica Content of Diatoms on Protozoan Grazing. *Frontiers in Marine Science*, *4*(June). https://doi.org/10.3389/fmars.2017.00202